# Single-top production at linear $e^-e^+$ colliders

Angel Escamilla, Antonio O. Bouzas,* and F. Larios
*Departamento de Física Aplicada, CINVESTAV-Mérida, Apartado Postal 73-Cordemex, 97310 Mérida, Yucatán, México*

(Received 7 December 2017; published 20 February 2018)

We study single-top production at linear lepton colliders with $\sqrt{s} = 0.5$, 1, and 3 TeV. A preliminary analysis shows that despite the large $t\bar{t}$ background at $\sqrt{s} = 0.5$ and 1 TeV it is possible to obtain a good sensitivity to the $tbW$ vertex, even more so at 3 TeV when single top becomes the dominant mode of production. Concerning the four-dimension six operators involved, two of them simultaneously generate $ttZ$ couplings and their sensitivity decreases with energy. The opposite is true for the other two operators. Single-top production at these machines is also useful to probe charged-current four-fermion operators $e\nu bt$, some of which are related to $tbW$ operators through the equations of motion.

DOI: 10.1103/PhysRevD.97.033004

## I. INTRODUCTION

Future linear lepton colliders such as the International Linear Collider (ILC) [1–5] and the Compact Linear Collider (CLIC) [6,7] have the top quark as one of their main areas of research. In particular, an extensive effort based on the dimension 6 operators [8] of the Standard Model Effective Field Theory is being developed for the top quark physics program at these colliders as well as at the LHC [9]. For the LHC, significant limits have been obtained when the effective couplings enter in loop-level [10–12] as well as tree-level processes [13,14], and many experimental measurements can be found in the literature, for $t\bar{t}$ production, $W$ helicity in top quark decay, rare top decays, same-sign tops production, and single-top, mono-top, and multiple-top production [15].

In the context of top quark production in $e^-e^+$ colliders, so far most of the interest has been placed on $t\bar{t}$ and $t\bar{t}H$ production at the ILC for beam energies of $\sqrt{s} = 0.5$ and 1 TeV [16], and very few studies have been done on single-top production [17–21]. It is now known that $ttZ(\gamma)$ couplings will be far better probed in this machine than at the LHC [22,23]. However, with respect to the $tbW$ coupling, the LHC is already providing very strong limits through single-top production and $W$ helicity in top decays [24]. In contrast, $t\bar{t}$ production at the linear collider has very little sensitivity to $tbW$ even for angular distributions of decay products [25]. To date, there is no study on the potential of single-top production in $e^-e^+$ collisions to probe the effective $tbW$ coupling. This is one of the goals of this paper: to find out what is the sensitivity to this coupling and how it compares with the potential of $e^+e^- \to t\bar{t}$ as well as the LHC. Furthermore, we also study the sensitivity to four-fermion operators $e\nu bt$ relevant to this process.

We refer in this study to the basis of dimension-6, $\mathrm{SU}(3) \times \mathrm{SU}(2) \times \mathrm{U}(1)$ gauge-invariant operators provided in [8]. In Tables I and II we show the flavor-diagonal operators in that basis that are relevant to top quark production at the ILC and CLIC. The notation used here is standard: $\tau^I$ are the Pauli matrices, $\varphi$ is the Standard Model (SM) Higgs doublet with $\tilde{\varphi} = i\tau^2\varphi^*$, $q_L$ is the third-generation left-handed SU(2) doublet, $t_R$ and $b_R$ are the right-handed SU(2) singlets. The covariant derivative is defined as $D_\mu\varphi = \partial_\mu\varphi - ig/2\tau^I W^I_\mu\varphi - ig'/2B_\mu\varphi$. As described in more detail below, we will follow the operator normalization used in [11,13].

The basis operators generating couplings of the top quark to the gauge bosons are displayed in Table I. As shown there, there are three operators that only generate neutral current (NC) $ttZ$ and $tt\gamma$ vertices, and two that generate both charged-current (CC) and NC couplings. For these five operators, the ILC $t\bar{t}$ process can indeed surpass the potential of the LHC [23,26]. The remaining two operators in Table I generate solely CC $tbW$ effective couplings that cannot be sensitively probed by top-pair production. In this paper, we discuss whether the single-top production mode at the linear colliders would be able to give bounds for the two purely CC operators similar to or more stringent than the LHC and how the limits on the two mixed NC-CC operators from single-top compare to those from top-pair production.

We parenthetically point out here that, strictly speaking, the distinction between NC operators and CC operators that

*Corresponding author.
abouzas@fis.mda.cinvestav.mx

*Published by the American Physical Society under the terms of the Creative Commons Attribution 4.0 International license. Further distribution of this work must maintain attribution to the author(s) and the published article's title, journal citation, and DOI. Funded by SCOAP³.*

TABLE I. Operators relevant for top production at ILC. Top-gauge boson. Indices 33 stand for third-generation quarks.

| $ttZ + ttA$ | $ttZ + ttA + tbW$ | $tbW$ |
|---|---|---|
| $O_{\varphi q}^{(1)33} = \varphi^\dagger i\bar{D}_\mu \varphi \bar{q}_L \gamma^\mu q_L$ | $O_{\varphi q}^{(3)33} = \varphi^\dagger i\bar{D}_\mu^I \varphi \bar{q}_L \tau^I \gamma^\mu q_L$ | $O_{\varphi ud}^{33} = \tilde{\varphi}^\dagger i D_\mu \varphi \bar{t}_R \gamma^\mu b_R$ |
| $O_{\varphi u}^{33} = \varphi^\dagger i\bar{D}_\mu \varphi \bar{t}_R \gamma^\mu t_R$ | $O_{uW}^{33} = \bar{q}_L \sigma^{\mu\nu} t_R \tau^I \tilde{\varphi} W_{\mu\nu}^I$ | $O_{dW}^{33} = \bar{q}_L \sigma^{\mu\nu} b_R \tau^I \varphi W_{\mu\nu}^I$ |
| $O_{uB}^{33} = \bar{q}_L \sigma^{\mu\nu} t_R \tilde{\varphi} B_{\mu\nu}$ | … | … |

TABLE II. Four-fermion operators relevant for top production at ILC. Indices 13 stand for first-family leptons and third-family quarks.

| $eett$ | $eett + e\nu tb$ | $e\nu tb$ |
|---|---|---|
| $O_{\ell q}^{(1)13} = \bar{\ell}_L \gamma_\mu \ell_L \bar{q}_L \gamma^\mu q_L$ | $O_{\ell q}^{(3)13} = \bar{\ell}_L \gamma_\mu \tau^I \ell_L \bar{q}_L \gamma^\mu \tau^I q_L$ | $O_{\ell edq}^{13} = \bar{\ell}_L e_R \bar{b}_R q_L$ |
| $O_{eu}^{13} = \bar{e}_R \gamma_\mu e_R \bar{t}_R \gamma^\mu t_R$ | $O_{\ell equ}^{(1)13} = \bar{\ell}_L^j e \epsilon_{jk} \bar{q}_L^k t$ | … |
| $O_{\ell u}^{13} = \bar{\ell}_L \gamma_\mu \ell_L \bar{t}_R \gamma^\mu t_R$ | $O_{\ell equ}^{(3)13} = \bar{\ell}_L^j \sigma_{\mu\nu} e_R \epsilon_{jk} \bar{q}_L^k \sigma^{\mu\nu} t_R$ | … |
| $O_{qe}^{13} = \bar{q}_L \gamma_\mu q_L \bar{e}_R \gamma^\mu e_R$ | … | … |

are sensitive to the top-pair and the single-top processes separately is not fully clear-cut. Indeed, it has been pointed out that off-shell effects in top-pair production can indeed bring sensitivity to the $tbW$ coupling and, in particular, be used to measure the top quark width with great accuracy [27,28], which argues in favor of the notion that the potential of the ILC and CLIC machines in studying top quark physics will go beyond the context of on-shell $t\bar{t}$ production.

As has been pointed out in [29], a consistent analysis of top-gauge boson operators cannot exclude the effects of four-fermion operators. Indeed, the choice of dimension 6 basis top-gauge boson operators implies that other operators of the same type are deemed redundant because of the equations of motion [8]. These equations of motion involve four-fermion operators that are chosen to appear in the list of independent operators and, therefore, must be included in the analysis if it is to be mathematically consistent and model independent.

The basis operators generating four-fermion vertices involving the top quark are shown in Table II. As with the quark-gauge boson operators, we focus on operators containing only third-generation quarks and, in the case of four-fermion operators, first-family leptons. As seen in Table II, there are four operators generating purely $eett$ vertices that are related only to NC $t\bar{t}$ production. We will not consider them in this paper; a recent study on the ILC potential to probe them can be found in [30]. Another goal of this paper is to obtain the limits set by single-top production on the remaining four operators in the table, which generate CC-type $e\nu tb$ couplings relevant to that process.

This article is organized as follows. In Sec. II, we discuss in detail the SM process of single-top production and decay at an $e^-e^+$ collider, as well as its reducible and irreducible backgrounds and the role of beam polarizations. In Sec. III, we review the flavor-diagonal effective operators relevant to single-top production and discuss the recent LHC results on effective top-gauge boson couplings and the projected sensitivity of top-pair production at the ILC to those couplings, which set the context against which single-top production at ILC and CLIC must be analyzed. In Sec. IV, we obtain bounds on the effective couplings from the single-top total cross section, both at the individual-coupling level and for pairs of couplings, at $\sqrt{s} = 0.5$, 1, and 3 TeV for certain ranges of experimental uncertainties at each energy. Finally, in Sec. V we present our conclusions.

## II. TOP QUARK PRODUCTION AT AN $e^+e^-$ COLLIDER

To better understand why we have chosen the single-top process defined below in (2), let us review the context of top-pair and single-top production in an $e^+e^-$ collider. Unlike the LHC, $t\bar{t}$ production at the ILC is generated by the electroweak interaction and becomes an irreducible background for single-top production. Single-top production can be hard to distinguish from $e^+e^- \to t\bar{t}$, particularly near the threshold region. This intermingling makes off-shell effects in top-pair production sensitive to the $tbW$ vertex. Therefore, it can be used to probe the $tbW$ vertex and the top width [27,28]. At tree level, $\sigma(e^+e^- \to t\bar{t})$ is given by just two diagrams ($s$-channel $Z$ and $\gamma$). At $\sqrt{s} = 0.5$ TeV, the cross section is about 550 fb, with an increase of about 15% when QCD corrections are included [31]. If we require one of the top quark lines to be about 20 GeV away from the resonance so as to obtain

single-top events, the contribution from these two diagrams yields $\sigma(e^+e^- \to tt^* \to t\bar{b}W^- + \bar{t}bW^+) \simeq 20$ fb. This does not mean that $tt^*$ is the main source of single-top production. If we consider the $t\bar{b}W^-$ final state, with no Cabibbo-Kobayashi-Maskawa (CKM) mixing, we will find that there are a total of seven diagrams, with only two of them corresponding to $tt^*$, and that the cross section is actually $\sigma(e^+e^- \to t\bar{b}W^- + \bar{t}bW^+) \simeq 50$ fb. At this level, one can ask what are the possible decay channels and the most interesting ones. We should bear in mind that the final states coincide with the well known $t\bar{t}$ decay channels. The dileptonic channel, with the 4.5% fraction of about 2.3 fb, would yield about 2300 events with a luminosity of 1 $\text{ab}^{-1}$ before cuts. This is actually a very rough estimate; let us consider specifically $e^+e^- \to \bar{b}\mu^-\bar{\nu}_\mu be^+\nu_e$ that with a 1.1% fraction we would expect to contribute with about 0.55 fb. It turns out that this process in particular has 438 diagrams, indeed most of them with no $t$ lines. After imposing a cut on the invariant $M_{b\bar{b}}$ to be away from the $Z$ and Higgs boson resonances, the cross section reduces to just about 0.2 fb [20]. The dileptonic channel thus seems to yield rather poor statistics. Let us now consider the semileptonic mode, with final states $\ell^-\bar{\nu}\,\bar{b}\,bjj$ or $\ell^+\nu b\bar{b}jj$. Whether the lepton is an electron or a muon we now expect to have about a $2 \times 7.2\%$ fraction that is about $2 \times 3.6$ fb for each possibility $\ell = e, \mu$. However, if $e^\pm$ is the lepton in the final state, one desirable feature arises: $t$-channel diagrams appear. In $t$-channel diagrams, there are no $ttZ(\gamma)$ vertices and the sensitivity goes only to the $tbW$ coupling. From [18], we find that the actual cross section for $e^+e^- \to t\bar{b}e^-\bar{\nu}_e$ is about 3 fb, where the invariant mass of the $be^-\bar{\nu}_e$ system is at least 20 GeV away from the top quark resonance. With a 67% fraction of the hadronic decay, we then expect to have a total of 4 fb for the semileptonic mode with the electron. Kinematic cuts will still reduce this number significantly, as we shall see below, but yet enough cross section will survive that would yield good statistics. This is the final state of interest for this study: two $b$ jets, two light quarks, an electron or positron and its neutrino.

### A. Semileptonic signal process and irreducible background

The set of Feynman diagrams for top quark production and decay in $e^-e^+$ collisions in the SM in the semileptonic channel is a subset of those for the six-fermion processes

$$e^-e^+ \to q_u\bar{q}_d b\bar{b}e^-\bar{\nu}_e + \bar{q}_u q_d b\bar{b}e^+\nu_e, \quad \text{with} \quad q_u = u, c, \quad q_d = d, s. \tag{1}$$

The final states (1) can be reached through two different top production processes, one followed by hadronic top decay

$$e^-e^+ \to \begin{cases} t\bar{b}e^-\bar{\nu}_e, & t \to q_u\bar{q}_d b, \\ \bar{t}be^+\nu_e, & \bar{t} \to \bar{q}_u q_d \bar{b}, \end{cases} \tag{2a}$$

and the other one followed by leptonic decay

$$e^-e^+ \to \begin{cases} t\bar{b}\bar{q}_u q_d, & t \to e^+\nu_e b, \\ \bar{t}bq_u\bar{q}_d, & \bar{t} \to e^-\bar{\nu}_e\bar{b}. \end{cases} \tag{2b}$$

The process (2a) has been studied in [17,18] at the top production level ($e^-e^+ \to t\bar{b}e^-\bar{\nu}_e$). Here, we extend that study to include top decay and the process (2b).

The Feynman diagrams for the process (2) are shown in Figs. 1–4 for the final states containing $e^-\bar{\nu}_e$. We set the electron mass $m_e = 0$, thus decoupling the electron from the Higgs field. We take into account only Cabibbo mixing in our computations, since third-generation mixing can be safely neglected for our purposes. Thus, in (2) we have $(q_u, \bar{q}_d) = (u, \bar{d}), (u, \bar{s}), (c, \bar{d}), (c, \bar{s})$. With these considerations, the six topologies corresponding

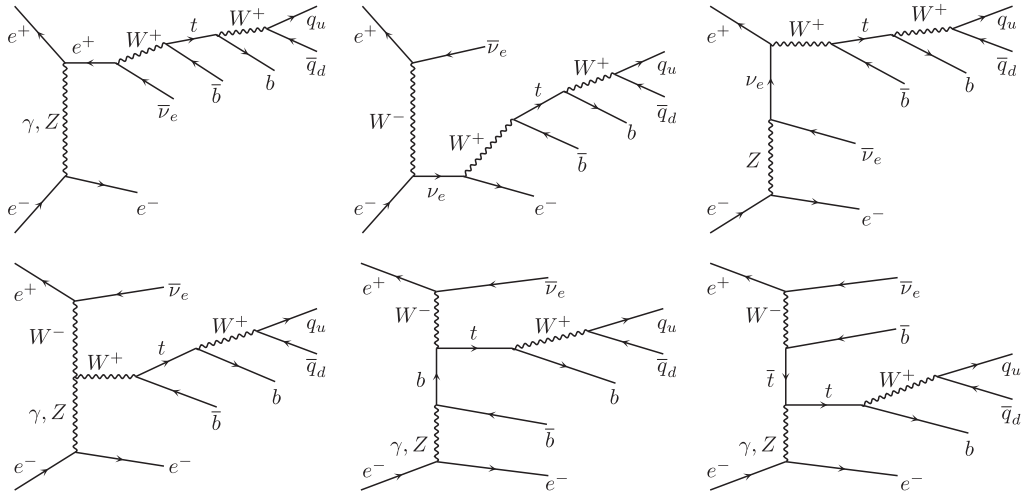


FIG. 1. Unitary gauge Feynman diagrams for single-top production in $e^-e^+$ collisions with $t$-channel vector boson exchange.

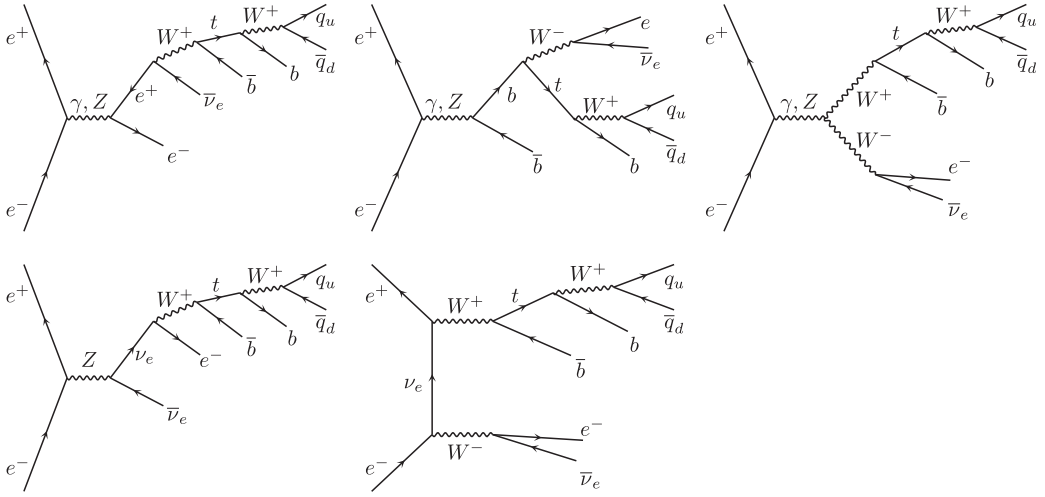


FIG. 2. Unitary gauge Feynman diagrams for single-top production in $e^-e^+$ collisions with $s$-channel vector boson exchange and hadronic top decay.

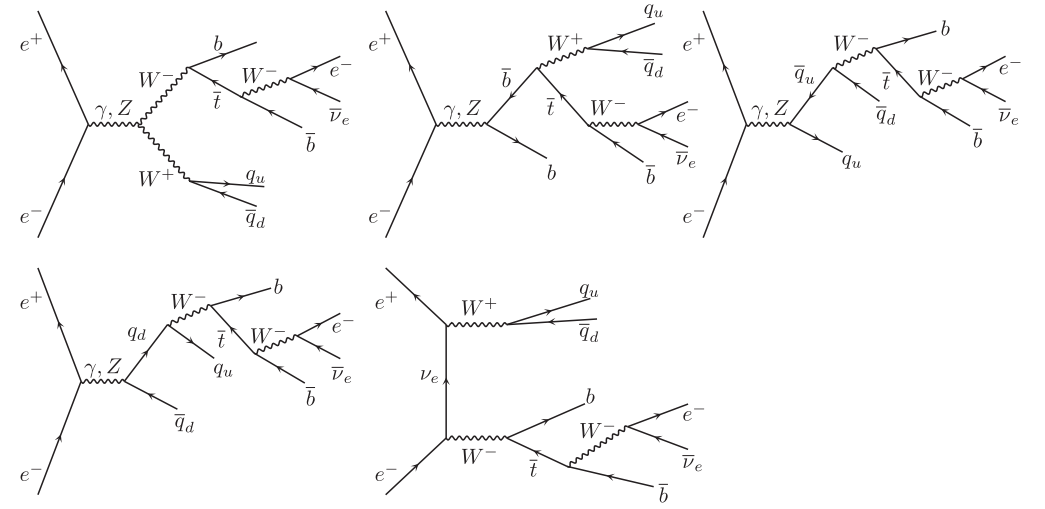


FIG. 3. Unitary gauge Feynman diagrams for single-top production in $e^-e^+$ collisions with $s$-channel vector boson exchange and leptonic top decay.

to $t$-channel vector boson exchange in Fig. 1 lead to 40 Feynman diagrams. Notice that those diagrams involve only hadronic top decay. The $s$-channel vector boson exchange diagrams with one internal top line decaying hadronically are given by the five topologies in Fig. 2, corresponding to 32 diagrams. The $s$-channel diagrams with one top decaying leptonically are given by the five topologies in Fig. 3, leading to 36 diagrams. Finally, Fig. 4 shows one topology, corresponding to eight diagrams for $s$-channel vector boson exchange with two internal top lines, which contribute to single-top production when one top line is on its mass shell and the other one is off shell. We have, then, a total of 116 diagrams for semileptonic single-top production and decay in the SM with Cabibbo mixing, in the $e^-\bar{\nu}_e$ channel. If full CKM mixing is taken into account, the number of diagrams doubles to 232, since the additional diagrams with third-generation mixing can be obtained from the ones without it by just exchanging the $\bar{q}_d$ and $\bar{b}$ final-state lines in each diagram.

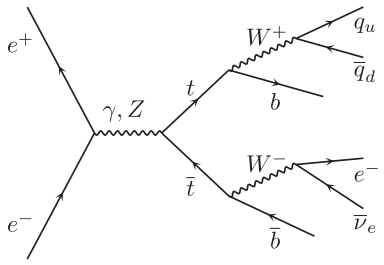


FIG. 4. Unitary gauge Feynman diagrams with a top-pair intermediate state. These diagrams contribute to single-top production when one top line is on shell and the other is off shell.

We consider the processes (2), given by the Feynman diagrams in Figs. 1–4, restricted to the following phase-space regions

$$\begin{aligned}
&\text{single-top hadronic}: && m(be\nu) \notin I_t \text{ and } m(bjj) \in I_t,\\
&\text{single-top leptonic}: && m(be\nu) \in I_t \text{ and } m(bjj) \notin I_t,\\
&\text{single top}: && (m(be\nu) \in I_t \text{ and } m(bjj) \notin I_t)\\
& && \text{or } (m(be\nu) \notin I_t \text{ and } m(bjj) \in I_t),\\
&\text{top pair}: && m(be\nu) \in I_t \text{ and } m(bjj) \in I_t,\\
&\text{off-shell}t: && m(be\nu) \notin I_t \text{ and } m(bjj) \notin I_t, \qquad (3)
\end{aligned}$$

where $I_t$ is a mass interval around the top mass, $I_t = (132, 212)$ GeV, and $m(be\nu)$, $m(bjj)$ refer to the invariant mass of the three-particle sets in the final state that can originate from a top decay. The single-top region in (3) corresponds to the process we are interested in, or "signal" process. The top-pair region in (3) refers to the production of an on-shell top pair, whereas the line labeled "off-shell $t$" corresponds to the phase-space region where no on-shell top is produced. Figure 5 displays the dependence on $\sqrt{s}$ of the total cross sections for the processes (2) restricted to the regions (3), with minimal phase-space cuts [see (5) below]. Also shown in the figure are the cross sections for the processes with $\mu^\mp$ final states, whose diagrams are given by those in Figs. 2–4 with the replacement $e, \nu_e \to \mu, \nu_\mu$. The cross sections for the muonic final states are equal to those for the process (2) restricted to the $s$ channel only, so that they illustrate the role of the $s$ channel in (2).

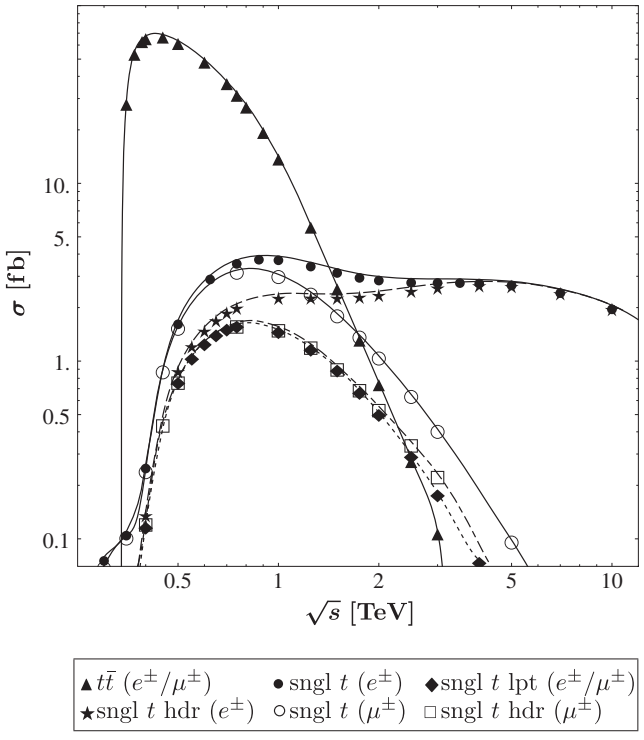


FIG. 5. Total cross section dependence with $\sqrt{s}$ for the single-top and top-pair production processes (3) with minimal phase-space cuts (5). Also shown are processes with $\mu\nu_\mu$ in the final state, which proceed only through the $s$-channel diagrams in Figs. 2–4.

The irreducible background to single-top production consists of all processes (1) not proceeding through the on-shell production of a single top. We distinguish three contributions to the irreducible background: (i) top-pair production, arising from the diagrams in Fig. 4 with both top lines on shell, (ii) off-shell top processes, comprising the diagrams in Figs. 1–4 with all internal top lines off shell, and (iii) no-top processes originating from all Feynman diagrams for (1), not containing any top quark propagator. It is clear by definition that there can be no interference between the processes (i) and (ii), and the interference between (i) and (iii) turns out to be suppressed, as discussed below. Therefore, it is appropriate to adopt the convention to refer to the contributions (ii) and (iii) together as irreducible background and to (i) as a separate top-pair production background.

For the process (1), with Cabibbo mixing and for the $e^-\bar{\nu}_e$ channel, there are 2064 diagrams without internal $t$ lines (1808 with six electroweak vertices, 256 with four electroweak vertices, and two strong ones). As we discuss in more detail below, at ILC-CLIC energies, 90% of the irreducible background cross section stems from the $WH$ and $WZ$ associated production processes

$$e^-e^+ \to W^+He^-\bar{\nu}_e, \qquad W^+ \to q_u\bar{q}_d, \qquad H \to b\bar{b}, \tag{4a}$$

$$e^-e^+ \to W^+Ze^-\bar{\nu}_e, \qquad W^+ \to q_u\bar{q}_d, \qquad Z \to b\bar{b}, \tag{4b}$$

and their charge conjugates. The process (4a) involves 96 Feynman diagrams and (4b) 320, for a total of 416 diagrams. In the computation of the irreducible background described below, however, we take into account the full process (1).

### B. Phase-space cuts and event selection

We compute the tree-level cross sections for single-top production and decay, and for the background processes, with the matrix-element Monte Carlo program MadGraph5_aMC@NLO (henceforth MG5) version 2.3 [32]. In all cases, we set $m_t = 172$ GeV, $m_b = 4.7$ GeV, $m_c = 1.27$ GeV, $m_Z = 91.19$ GeV, $m_W = 79.82$ GeV, $m_h = 125$ GeV, $\alpha(m_Z) = 1/132.507$, $G_F = 1.1664 \times 10^{-5}$ GeV$^{-2}$, and $\alpha_S(m_Z) = 0.118$. The masses of the lighter quarks, $e$ and $\mu$ are set to vanish, and the Higgs vacuum-expectation value $v = 246.22$ GeV. Furthermore, we take into account Cabibbo mixing with

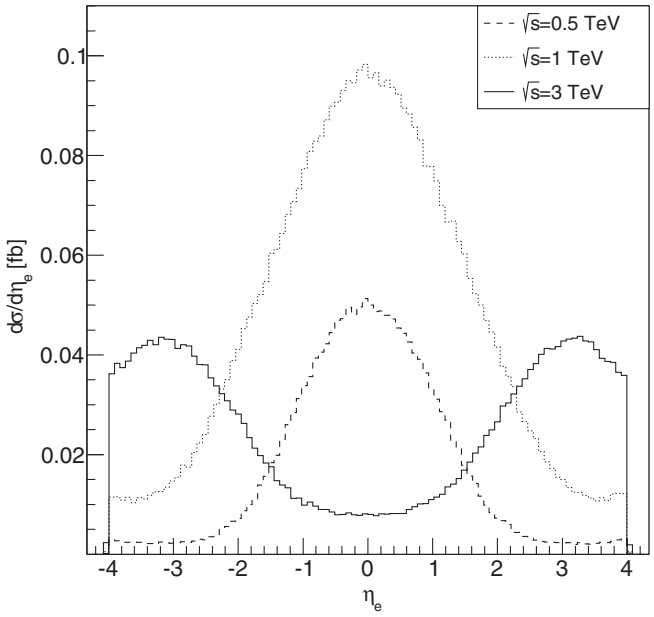


FIG. 6. Differential cross sections for the $e^{\mp}$ pseudorapidity for the signal process (2) with the cuts $A_0$, (5), and $C_0$, (6), normalized to total cross section (see Table III).

$\theta_c = 0.228$. For event analysis we use ROOT version 5.34 [33].

In order to make the cross section well defined and to improve the signal-to-background ratio, we apply several phase-space cuts discussed in detail in what follows. We impose minimal centrality and isolation cuts in the form

$$A_0\colon\ |\eta(e)| < 4, \qquad |\eta(j)| < 3, \qquad \Delta R_{\rm ch} > 0.5, \tag{5}$$

where $\eta(e)$ refers to the pseudorapidity of the final-state electron or positron, $\eta(j)$ to that of the jets, and $\Delta R_{\rm ch}$ to the distance in the $\eta - \phi$ plane between any pair of charged particles. We assume that the central detector system covers the central region $|\eta| < 3$–$3.5$ and the forward detectors cover the region $3 < |\eta| < 4$, as is expected to be the case at the ILC-CLIC [5,6]. As shown in Fig. 6, the cut on $\eta(e)$ is substantially more restrictive at the CLIC energy than at ILC's. This is a consequence of the fact that, at $\sqrt{s} = 3$ TeV, the process (2) occurs mostly through the $t$-channel vector boson exchange diagrams of Fig. 1, while at the ILC, the $s$-channel diagrams of Figs. 2–4 dominate, as shown in Fig. 5. The cut on $\Delta R = \sqrt{\Delta\eta^2 + \Delta\varphi^2}$ in (5) is an isolation cut setting the minimal distance between any two charged particles in the final state.

The reducible background to the process (2), which is studied in more detail below in Sec. II D, consists of final states with four jets, an electron or positron, and $\not{E}_\perp$, with the number of $b$ jets $N_b \neq 2$. Such final states contain pairs of massless partons, light quarks or gluons, which lead to infrared singularities. In order to avoid those singularities, we require the final-state jets to satisfy the condition

TABLE III. Effect of the phase-space cuts (5)–(10) on the total cross section for the process (2) and its subprocesses (3), and on the irreducible background. The $b$-tagging efficiency and mistagging probabilities involved in $C_1$ are given in the text under Eq. (7).

| $\sigma$ (fb), $\sqrt{s} = 0.5$ TeV | | | | | |
|---|---|---|---|---|---|
| | sngl-h | sngl-l | sngl | pair | irr.bkg. |
| $A_0$ | 0.93 | 0.79 | 1.72 | 62.28 | 2.09 |
| $C_0$ | 0.85 | 0.72 | 1.58 | 58.07 | 1.78 |
| $C_1$ | 0.53 | 0.46 | 0.99 | 35.41 | 1.10 |
| $C_2$ | 0.53 | 0.46 | 0.99 | ⋯ | 0.47 |
| $C_3$ | 0.36 | 0.32 | 0.68 | ⋯ | 0.039 |
| $C_4$ | 0.34 | 0.29 | 0.63 | ⋯ | 0.026 |
| $\sqrt{s} = 1$ TeV | | | | | |
| $A_0$ | 2.42 | 1.53 | 3.93 | 14.09 | 4.50 |
| $C_0$ | 2.15 | 1.43 | 3.58 | 12.94 | 3.13 |
| $C_1$ | 1.31 | 0.89 | 2.29 | 7.87 | 1.94 |
| $C_2$ | 1.31 | 0.89 | 2.29 | ⋯ | 1.07 |
| $C_3$ | 1.06 | 0.78 | 1.85 | ⋯ | 0.074 |
| $C_4$ | 0.99 | 0.72 | 1.72 | ⋯ | 0.057 |
| $\sqrt{s} = 3$ TeV | | | | | |
| $A_0$ | 2.77 | 0.18 | 2.95 | 0.12 | 11.25 |
| $C_0$ | 1.90 | 0.16 | 2.06 | 0.096 | 7.15 |
| $C_1$ | 1.16 | 0.099 | 1.26 | 0.059 | 4.43 |
| $C_2$ | 1.16 | 0.099 | 1.26 | ⋯ | 1.40 |
| $C_3$ | 0.96 | 0.096 | 1.06 | ⋯ | 0.060 |
| $C_4$ | 0.93 | 0.087 | 1.02 | ⋯ | 0.045 |

$$C_0\colon\ m(j,j') > \begin{cases} 60\ \text{GeV} & \text{if } \sqrt{s} = 3\ \text{TeV} \\ 40\ \text{GeV} & \text{if } \sqrt{s} = 1\ \text{TeV} \\ 30\ \text{GeV} & \text{if } \sqrt{s} = 0.5\ \text{TeV}, \end{cases} \tag{6}$$

where $m(j,j')$ refers to the mass of any pair of partons in the final state. As shown in Table III, the restriction $C_0$ cuts about 35% of the irreducible background cross sections both at ILC and CLIC energies, and it cuts about 10% of the signal at the ILC and 30% at the highest CLIC energy. In Fig. 7, we display several mass differential cross sections computed with the cuts (5) and (6), for the signal and irreducible background at $\sqrt{s} = 1$ TeV. At the other energies, 0.5 and 3 TeV, the distributions are qualitatively similar. The distributions of the $b$-pair mass $m(b\bar{b})$ and the light-jet pair $m(q\bar{q})$ for the irreducible background [dotted lines in Figs. 7(a) and (b), respectively] are seen to be dominated by the $Z$, $h$ peaks and $W$ peak, respectively, as expected from the main irreducible background processes (4). For instance, at $\sqrt{s} = 3$ TeV, the total cross section for (4) with the cuts $A_0$ and $C_0$ is found to be 6.57 fb, amounting to 92% of that of the total irreducible background, 7.15 fb, as given in Table III.

To suppress the reducible background, we require the final state to contain exactly two $b$-tagged jets

$$C_1\colon\ N_b = 2. \tag{7}$$

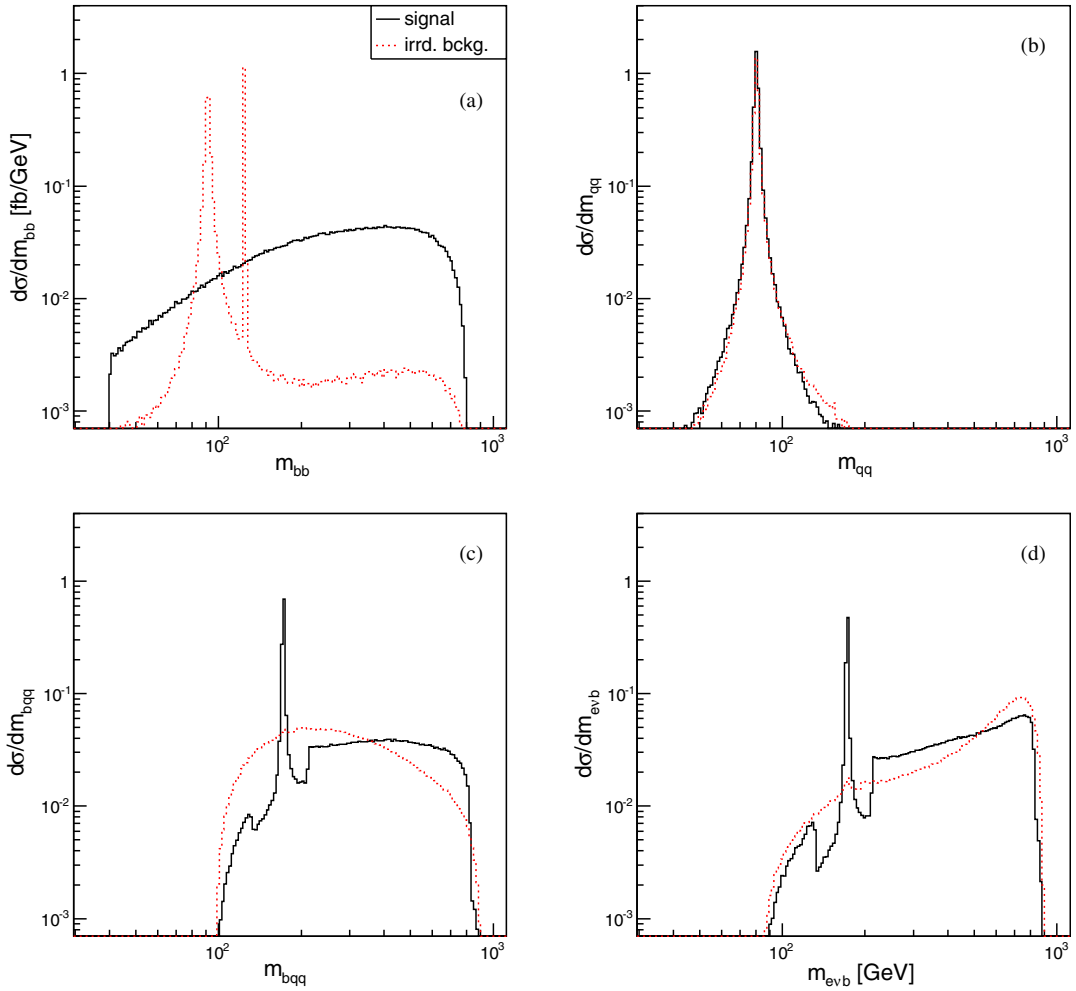


FIG. 7. Differential cross sections for the signal process (2) and irreducible background (irrd. bckg.) at $\sqrt{s} = 1$ TeV and with the cuts $A_0$, (5), and $C_0$, (6). All differential cross sections are normalized to total cross section: 3.58 fb for the signal and 3.13 fb for the background processes. With the notation of Eq. (8), the independent variables are (a) $m(J_0, J_1)$, (b) $m(J_1, J_2)$, (c) $m(J_1, J_2, J_3)$, (d) $m(J_0, e, \nu)$.

We assume the $b$-jet tagging efficiency to be $\eta_b = 80\%$ and the mistagging probabilities to be $p_c = 10\%$ for $c$ jets and $p_q = 1\%$ for the lighter jets. These are realistic values, consistent with the efficiencies currently achieved by LHC detectors [34]. In our analysis, we simulate $b$ tagging by relabeling $b$ quarks as lighter ones with 20% probability and by relabeling as $b$ quarks $c$ quarks with 10% probability and lighter partons with 1% probability. Thus, cut (7) results in the signal and irreducible background cross sections being reduced to about 61% of their value. The cut $C_1$ plays an important role in rejecting the reducible background, as discussed in detail below in Sec. II.D.

Most of the rejection of the irreducible background, and of the reducible background events remaining after cut (7), is achieved by requiring that each event must contain the decay products of exactly one on-shell top quark, as described by the "single-top" line in (3). We denote the four jets in the final state by $J_{0,\ldots,3}$, with $J_{0,1}$ the two $b$-tagged jets and $J_{2,3}$ the two light jets, the latter ones in no particular order. In events with a hadronically decaying top, we denote the promptly produced $b$ jet as $J_0$ and the $b$ jet from top decay as $J_1$, and for leptonic top decays we denote the prompt $b$ jet as $J_1$ and the $b$ jet from top decay as $J_0$. Thus, with this convention and with the notation introduced in (3), the phase-space cut for single-top events can be written as

$$C_2\colon\ (m(J_0, e, \nu) \in I_t \text{ and } m(J_1, J_2, J_3) \notin I_t) \quad \text{or}$$
$$(m(J_0, e, \nu) \notin I_t \text{ and } m(J_1, J_2, J_3) \in I_t), \tag{8}$$

where the first parenthesis corresponds to leptonically decaying and the second to hadronically decaying top quarks. In Fig. 7(c), the differential cross section for the invariant mass $m(b, j, j)$ for the signal process (solid line) corresponds to $m(J_1, J_2, J_3)$, and in Fig. 7(d), $m(b, e, \nu)$ corresponds to $m(J_0, e, \nu)$. For the irreducible background, the distributions of $m(b, j, j)$ and $m(b, e, \nu)$ obtained with each one of the two $b$ quarks in the final state are essentially identical.

The irreducible background contains a substantial combinatorial component satisfying (8), as is apparent from Fig. 7(c) where the distribution of $m(b,q,q)$ is seen to contain a significant number of events under the top mass peak. This yields a sizable irreducible background cross section even after the cut $C_2$ has been applied, as shown in Table III. Since most of the irreducible background consists of processes (4) in which the $b\bar{b}$ pair comes from $Z$ or $h$ decay, we are led to introduce the cut

$$C_3: \begin{cases} m(J_0,J_1) > 130 \text{ GeV} & \text{if } \sqrt{s} \geq 1 \text{ TeV}, \\ m(J_0,J_1) > 130 \quad \text{or} \quad m(J_0,J_1) < 70 \text{ GeV} & \text{if } \sqrt{s} = 0.5 \text{ TeV}, \end{cases} \tag{9}$$

to further suppress the remaining irreducible background. Finally, we require that the two light jets be the decay products of an on-shell $W$ boson (cf. Figs. 1–4) and that the final state contains substantial $\not{E}_T$,

$$C_4: \ 60 \text{ GeV} < m(J_2,J_3) < 100 \text{ GeV} \quad \text{and}$$
$$\not{E}_T > 10 \text{ GeV}. \tag{10}$$

Cut $C_4$ provides some further suppression of the irreducible background without significantly affecting the signal.

The cumulative effect of the phase-space cuts (5)–(10) on signal and background is shown in Table III. The lines of this table labeled $C_4$ give the cross sections for the signal and irreducible background, including the effect of $b$-tagging efficiencies and all phase-space cuts. From those results, and assuming an integrated luminosity $L = 1$ ab$^{-1}$, we estimate the statistical uncertainty in the signal cross section $\sigma_{\text{sgn1}}$ to be 4.0%, 2.4%, and 3.1% at $\sqrt{s} = 0.5$, 1, and 3 TeV, respectively. The irreducible background is seen to amount to 4.1%, 3.3%, and 4.4% of $\sigma_{\text{sgn}}$, respectively, at the same three energies.

### C. Top-pair background

Table III shows that the top-pair production background is fully rejected by the cut $C_2$, but that is true only when measurement uncertainties are not taken into account. If we allow for the effect on the cut $C_2$ of measurement uncertainties in $m(J_1,J_2,J_3)$ and $m(J_0,e,\nu)$, however, a fraction of top-pair events would pass that cut. For reasonably small measurement uncertainties, we expect that fraction of events to be a relatively small fraction of the pair-production cross section. In the case of CLIC, in which the $t\bar{t}$ cross section is already very small compared to that of single top, this effect is expected to be of second order. At the ILC, however, top-pair production is substantially larger than single top, so that even a small fraction of these events can become a large background. In this section, we quantify the top-pair background to single-top production taking into account the top-mass reconstruction uncertainty.

A goal of the ILC and CLIC detectors is to achieve high enough jet energy and mass resolution to be able to separate the $W$ and $Z$ peaks in the dijet mass spectrum [5,6]. As shown in Fig. 2.6 of [6], for that purpose, the mass resolution $\sigma_m/m$ must be better than 5%, with good separation of the $W$ and $Z$ peaks obtained for $\sigma_m/m = 2.5\%$. Motivated by that observation, we assume that the top mass will be reconstructed from three jets at the ILC-CLIC with a relative uncertainty in the range 5–7.5%. In order to obtain a quantitative estimate of the effect of measurement uncertainties on the $t\bar{t}$ background, we randomly smear the reconstructed masses $m(J_1,J_2,J_3)$ and $m(J_0,e,\nu)$ before applying the cut $C_2$ to each top-pair production event. We assume those masses to be independently normal distributed with standard-deviation parameter $\sigma_m = \varepsilon_m m$, where $\varepsilon_m$ is the assumed relative uncertainty. For simplicity, we assume the same value of $\varepsilon_m$ for both $m(J_1,J_2,J_3)$ and $m(J_0,e,\nu)$. We carry out this randomized analysis of the $t\bar{t}$ event sample a few thousand times to obtain a statistical sample of the $t\bar{t}$ cross section after cuts $A_0$, $C_{0,\ldots,4}$. The resulting $\sigma_{t\bar{t}}$ distribution is strongly asymmetric with a long tail to the right, so we characterize it by the interval $(\langle\sigma_{t\bar{t}}\rangle, \langle\sigma_{t\bar{t}}\rangle + \Delta\sigma_{t\bar{t}})$.

At $\sqrt{s} = 3$ TeV, if we assume the top mass to be reconstructed with uncertainty $\varepsilon_m = 5\%$, the $t\bar{t}$ background turns out to be 0.48%–0.50% of the single-top cross section with all cuts, $A_0$, $C_{0,\ldots,4}$, as given in Table III. For $\varepsilon_m = 7.5\%$, we find the $t\bar{t}$ background to be 0.51%–0.79% of the single-top cross section. As expected, that background turns out to represent a small uncertainty at CLIC energy.

At $\sqrt{s} = 1$ TeV, for $\varepsilon_m = 5\%$, the $t\bar{t}$ background result is 1.6%–3.3% of the single-top cross section. For $\varepsilon_m = 7.5\%$, we get 3.5%–16.4%. We see that, for $\varepsilon_m$ less than 7.5%, the $t\bar{t}$ background is limited to about 15% of the single-top cross section, and for lower values near $\varepsilon_m \simeq 5\%$, that background can be somewhat less than 5%.

At $\sqrt{s} = 0.5$ TeV, for $\varepsilon_m = 5\%$, the $t\bar{t}$ background is 8.6%–17% of the single-top cross section. If $\varepsilon_m = 7.5\%$, we get 16.5%–50.5% for the $t\bar{t}$ background. These results are also not unexpected, since the $t\bar{t}$ cross section is large at the ILC at 0.5 TeV and can potentially swamp the single-top process. They also suggest, however, that the top-pair background can be limited to the range 10–30% for $\varepsilon_m$ less than 7% and to the range 10–20% if $\varepsilon_m$ is close to 5%.

### D. Reducible background

The reducible background to the single-top production process (2) is given by processes of the form

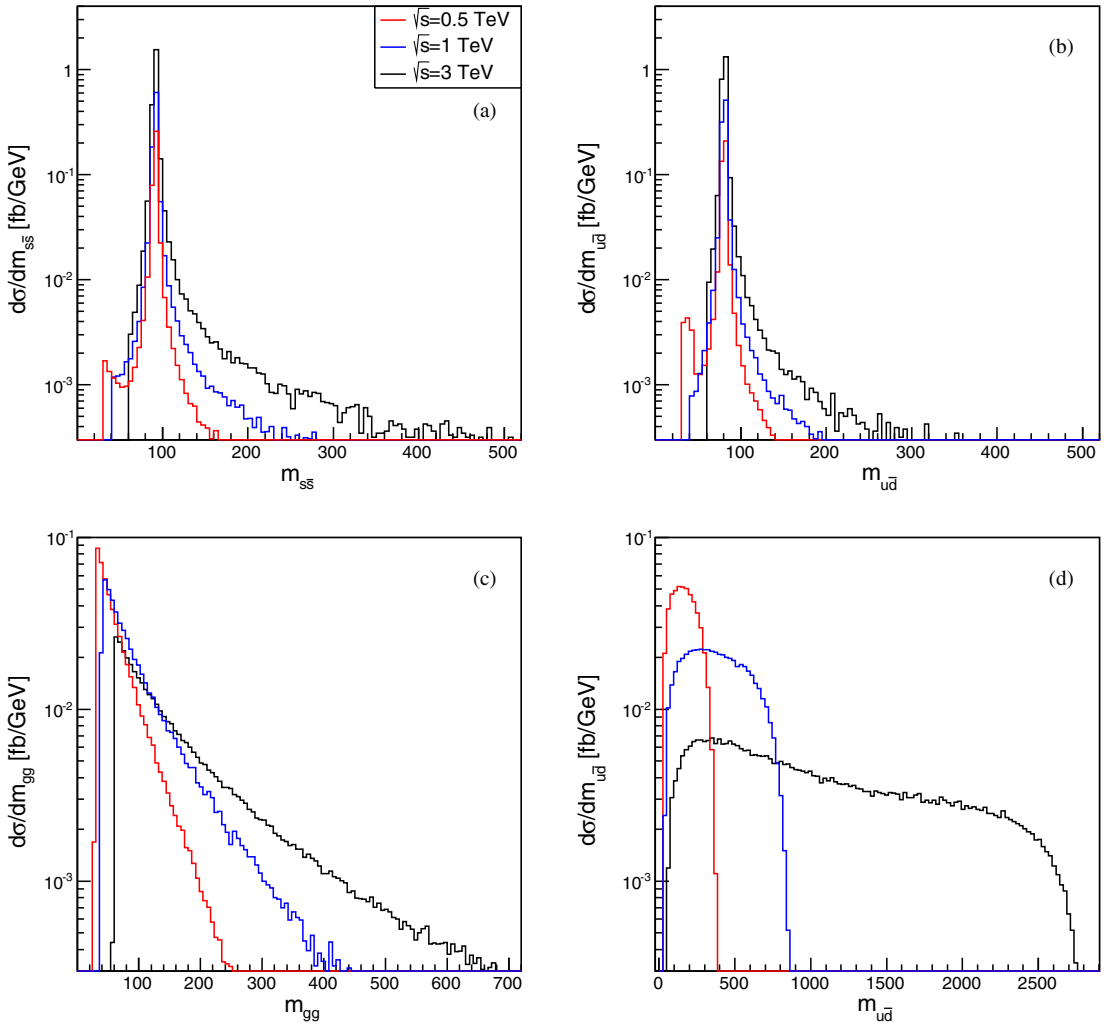


FIG. 8. Differential cross sections for the reducible background processes $e^-e^+ \to u\bar{d}s\bar{s}e^-\bar{\nu}_e$ (a),(b) and $e^-e^+ \to u\bar{d}gge^-\bar{\nu}_e$ (c),(d), with the cuts $A_0$, (5), and $C_0$, (6), normalized to total cross section.

$$e^-e^+ \to j_1j_2j_3j_4e^-\bar{\nu}_e + j_1j_2j_3j_4e^+\nu_e, \qquad (11)$$

with $j = u, d, c, s, b, g$ or their antiparticles. The number of $b/\bar{b}$ jets in (11) can be $N_b = 0$, 1, 3 (with $N_b = 2$ corresponding to the signal and irreducible background processes (1) and $N_b = 4$ being forbidden by electric charge conservation). Since the probability to mistag a final state (11) with $N_b \neq 2$ as one with $N_b = 2$ as in (1) depends on $N_b$ and on the number $N_c$ of $c/\bar{c}$ quarks, we have to consider separately the cases with different values of $N_b$, $N_c$.

For our computation of the reducible background, we adopt two-generation Cabibbo mixing, since the effects of third-generation mixing on cross sections are numerically inconsequential. This implies, in particular, that only processes (11) with $N_b = 0$ and without internal $t$ lines are possible. Indeed, explicit computation shows that the final states (11) with $N_b = 1$, 3, which can only occur through third-generation mixing, lead to cross sections of $\mathcal{O}(10^{-2}$ fb) at most even before the restrictive cuts $C_{1\ldots4}$ in Eqs. (7)–(10) are applied. For the same reason, equally negligible cross sections are obtained for diagrams with $N_b = 0$ with one or more internal $t$ lines.

The reducible background (11) contains a large number of subprocesses, whose detailed description is not needed for our purposes. With only two-generation mixing taken into account, it involves 15632 Feynman diagrams with $e^-\bar{\nu}_e$ final states. However, some general features of this background, with cuts $A_0$, $C_0$, are easily understood. With those cuts, the gluon final states $q_u\bar{q}_dgg$ are a minority fraction of the cross section. The final states $q_u\bar{q}_dq\bar{q}$ that dominate the cross section originate mostly from $WZ$ associated production, as seen from Fig. 8, in a similar way as the irreducible background.

We compute the reducible background cross section by applying the acceptance cuts $A_0$, (5), to particles with electric or color charge (i.e., to charged leptons, quarks, and gluons). The cut $C_0$, (6), is also required to make the cross section infrared finite. Simulation of light-parton mistagging is carried out, as discussed in the text below (7), by

TABLE IV. Effect of the phase-space cut (7) on the total cross section for the process (11). The $b$-tagging efficiency and mistagging probabilities involved in $C_1$ are given in the text under Eq. (7).

| $\sigma$ (fb), $\sqrt{s} = 0.5$ TeV | | | | |
|---|---|---|---|---|
| | $0_b0_c$ | $0_b1_c$ | $0_b2_c$ | $0_b3_c$ |
| $A_0$, $C_0$ | 1.71 | 1.72 | 0.38 | 0.38 |
| $C_1$ | $1.03 \times 10^{-3}$ | $5.43 \times 10^{-3}$ | $5.14 \times 10^{-3}$ | $1.11 \times 10^{-2}$ |
| $\sqrt{s} = 1$ TeV | | | | |
| | $0_b0_c$ | $0_b1_c$ | $0_b2_c$ | $0_b3_c$ |
| $A_0$, $C_0$ | 3.29 | 3.29 | 0.85 | 0.85 |
| $C_1$ | $2.04 \times 10^{-3}$ | $9.48 \times 10^{-3}$ | $1.12 \times 10^{-2}$ | $2.42 \times 10^{-2}$ |
| $\sqrt{s} = 3$ TeV | | | | |
| | $0_b0_c$ | $0_b1_c$ | $0_b2_c$ | $0_b3_c$ |
| $A_0$, $C_0$ | 6.85 | 6.82 | 2.00 | 1.98 |
| $C_1$ | $3.50 \times 10^{-3}$ | $1.98 \times 10^{-2}$ | $2.49 \times 10^{-2}$ | $5.35 \times 10^{-2}$ |

relabeling $c$ quarks as $b$ ones with probability $p_c = 0.1$ and lighter partons with probability $p = 0.01$. The resulting mistagging probabilities for processes (11) with $N_b = 0$ are given by

$$\begin{aligned} 0_b0_c: &\quad 6p^2q^2 &&= 5.88 \times 10^{-4}, \\ 0_b1_c: &\quad 3pp_cq^2 + 3p^2qq_c &&= 3.21 \times 10^{-3}, \\ 0_b2_c: &\quad p_c^2q^2 + 4pp_cqq_c + p^2q_c^2 &&= 1.34 \times 10^{-2}, \\ 0_b3_c: &\quad 3p_c^2qq_c + 3pp_cq_c^2 &&= 2.92 \times 10^{-2}, \end{aligned} \tag{12}$$

with $q = 1 - p$, $q_c = 1 - p_c$. The mistagged final states, containing two "fake" $b$ quarks, are then required to pass the cuts $C_{2\ldots4}$, as defined in (8)–(10), in the same way as the signal and irreducible background. The effects of cuts $A_0$, $C_{0,1}$ on the total cross sections are shown in Table IV. Notice that, at each energy, the cross sections corresponding to cut $C_1$ can be obtained by multiplying the results for the cuts $A_0$ and $C_0$ by the corresponding probabilities in (12), up to a small numerical uncertainty. As seen from the table, those cross sections are at most $\mathcal{O}(10^{-2}$ fb). After cuts $C_{2\ldots4}$ are applied, the resulting reducible background cross sections are at most $\mathcal{O}(10^{-3}$ fb) and therefore negligible.

### E. Beam polarization

The ILC baseline design supposes a polarization of the electron beam of at least 80% and 30% for the positron beam [4]. For CLIC, the baseline design assumes an electron beam polarization of 80% and an unpolarized positron beam [6]. In both accelerators, a later upgrade is foreseen that would increase the positron beam polarization to 60% [4,6]. In the study of single-top production, beam polarization may lead to a reduction of the measurement uncertainties, either by increasing the signal cross section, therefore reducing the statistical uncertainty, or by suppressing important backgrounds.

At $\sqrt{s} = 3$ TeV, the cross section uncertainties are dominated by the irreducible background and the statistical uncertainty (about 4.4% and 3.1%, respectively, as noted at the end of Sec. II B). The top-pair production background uncertainty is subdominant, as discussed in Sec. II C. The longitudinal beam polarization combinations that cause the signal cross section to increase or decrease have the same effect on the irreducible background, though not necessarily in the same amount. With longitudinal polarizations $(\mathcal{P}_{e^-}, \mathcal{P}_{e^+}) = (-90\%, 60\%)$, both the signal and irreducible background increase, leading to a statistical uncertainty of 2% and an irreducible background of 6.2%, thus worsening the overall uncertainty. For $(\mathcal{P}_{e^-}, \mathcal{P}_{e^+}) = (-90\%, -60\%)$, we get a statistical uncertainty of 3.2% and an irreducible background of 4.7%, and for $(\mathcal{P}_{e^-}, \mathcal{P}_{e^+}) = (90\%, 60\%)$, we get 4.4% and 4.5%, respectively; these cases show little change in the uncertainties with respect to the unpolarized case. Finally, for $(\mathcal{P}_{e^-}, \mathcal{P}_{e^+}) = (90\%, -60\%)$, the statistical uncertainty grows to 8% while the irreducible background decreases to 3.3%, for an overall uncertainty considerably worse than the unpolarized result. At this energy, therefore, we find that even the highest possible beam polarizations do not lead to a significant reduction in the cross section uncertainty with respect to the unpolarized case.

At $\sqrt{s} = 1$ TeV, assuming an integrated luminosity $L = 1$ ab$^{-1}$, we found in Sec. II B a statistical uncertainty of 2.4% and an irreducible background of 3.3%. As discussed in Sec. II C, top-pair production may be significantly larger than the irreducible background. Assuming the highest possible beam polarizations, we find that $(\mathcal{P}_{e^-}, \mathcal{P}_{e^+}) = (-90\%, 60\%)$ increases the signal cross section $\sigma_{\text{sgnl}}$ by a factor 2.72 relative to the unpolarized case, thus reducing the statistical uncertainty to 1.5%. The irreducible and top-pair production backgrounds increase by a factor of 2 and 2.24, respectively, so that $\sigma_{\text{irr}}/\sigma_{\text{sgnl}}$ decreases by 25% and $\sigma_{t\bar{t}}/\sigma_{\text{sgnl}}$ by 20% with respect to the unpolarized case. The polarizations $(\mathcal{P}_{e^-}, \mathcal{P}_{e^+}) = (-90\%, -60\%)$ also reduce the ratio $\sigma_{t\bar{t}}/\sigma_{\text{sgnl}}$, but by decreasing all cross sections. The signal cross section $\sigma_{\text{sgnl}}$ decreases by a factor 0.79,

thus slightly increasing the statistical uncertainty to 2.7%. The ratio $\sigma_{\rm irr}/\sigma_{\rm sgnl}$ remains unchanged and $\sigma_{t\bar{t}}/\sigma_{\rm sgnl}$ decreases by 25% with respect to the unpolarized case.

At $\sqrt{s} = 0.5$ TeV from Sec. II B, we get a statistical uncertainty of 4% and an irreducible background of 3.3% relative to the signal cross section $\sigma_{\rm sgnl}$. From Sec. II C, it is apparent that at this energy the $t\bar{t}$ production background strongly dominates the cross section uncertainty. The beam polarizations $(\mathcal{P}_{e^-}, \mathcal{P}_{e^+}) = (-90\%, 60\%)$ increases $\sigma_{\rm sgnl}$ by a factor of 2.7 and $\sigma_{t\bar{t}}$ by 2.2, thus leading to a decrease in $\sigma_{t\bar{t}}/\sigma_{\rm sgnl}$ of 20%. The polarizations $(\mathcal{P}_{e^-}, \mathcal{P}_{e^+}) = (-90\%, -60\%)$ decrease $\sigma_{\rm sgnl}$ by a factor 0.7 and $\sigma_{t\bar{t}}$ by 0.6, thus reducing $\sigma_{t\bar{t}}/\sigma_{\rm sgnl}$ by 20%.

Therefore, at ILC energies, we expect the highest beam polarizations to lead to a moderate reduction of single-top cross section uncertainties by 20%–25%. Lower polarizations would yield correspondingly smaller uncertainty reductions.

## III. EFFECTIVE OPERATORS FOR SINGLE-TOP PRODUCTION AT $e^-e^+$ COLLIDERS

The Lagrangian for the single-top production processes (2) is of the form

$$\mathcal{L} = \mathcal{L}_{\rm SM} + \frac{1}{\Lambda^2}\sum_{\mathcal{O}}(C_{\mathcal{O}}\mathcal{O} + \text{H.c.}) + \cdots, \tag{13}$$

where $\mathcal{O}$ denotes dimension 6 effective operators, $\Lambda$ is the new-physics scale, and the ellipsis refers to higher-dimensional operators. It will be convenient in what follows to express our results in terms of the modified dimensionless couplings

$$\bar{C}_{\mathcal{O}} = C_{\mathcal{O}}\frac{v^2}{\Lambda^2}, \tag{14}$$

where $v$ is the Higgs-field vacuum expectation value. At tree level, the coupling constants $\bar{C}_{\mathcal{O}}$ are independent of the scale $\Lambda$. We denote complex couplings as $\bar{C}_{\mathcal{O}} = \bar{C}_{\mathcal{O}r} + i\bar{C}_{\mathcal{O}i}$.

Throughout this paper, we use the dimension 6 effective operators from the operator basis given in [8]. However, we adopt the sign convention in the covariant derivatives and the operator normalization defined in [11], where a factor $y_t$ is attached to an operator for each Higgs field it contains and a factor $g$ ($g'$) is for each $W_{\mu\nu}$ ($B_{\mu\nu}$) field-strength tensor. We are interested in those operators that can contribute to single-top production at an $e^+e^-$ collider. There are operators with flavor changing couplings, but in this study, we will not consider them.

### A. Operators that generate $tbW$ couplings

There are four dimension 6 operators in the basis [8] that give rise to effective $tbW$ couplings: $O^{(3)}_{\varphi q}$, $O_{uW}$, $O_{\varphi ud}$, and $O_{dW}$, where we are omitting generation indices. The first two also generate NC couplings and are among the operators contributing to $e^+e^- \to t\bar{t}$. We combine operator $O^{(3)}_{\varphi q}$ with $O^{(1)}_{\varphi q}$ so as to eliminate the $bbZ$ neutral current term. Expanding these operators in physical fields we obtain

$$\begin{aligned}
O^{(-)33}_{\varphi q} &= O^{(3)33}_{\varphi q} - O^{(1)33}_{\varphi q} \\
&= \frac{y_t^2}{\sqrt{2}} g(v+h)^2 (W^+_\mu \bar{t}_L \gamma^\mu b_L + W^-_\mu \bar{b}_L \gamma^\mu t_L) \\
&\quad + y_t^2 \frac{g}{c_W}(v+h)^2 Z_\mu \bar{t}_L \gamma^\mu t_L, \\
O^{33}_{\varphi ud} &= \frac{y_t^2}{2\sqrt{2}} g(v+h)^2 W^+_\mu \bar{t}_R \gamma^\mu b_R, \\
O^{33}_{uW} &= 2y_t g(v+h)(\partial_\mu W^-_\nu + igW^3_\mu W^-_\nu)\bar{b}_L \sigma^{\mu\nu} t_R \\
&\quad + \sqrt{2} y_t g(v+h)(\partial_\mu W^3_\nu + igW^-_\mu W^+_\nu)\bar{t}_L \sigma^{\mu\nu} t_R, \\
O^{33}_{dW} &= 2y_t g(v+h)(\partial_\mu W^+_\nu + igW^+_\mu W^3_\nu)\bar{t}_L \sigma^{\mu\nu} b_R \\
&\quad - \sqrt{2} y_t g(v+h)(\partial_\mu W^3_\nu + igW^+_\mu W^-_\nu)\bar{b}_L \sigma^{\mu\nu} b_R.
\end{aligned} \tag{15}$$

The relation between the couplings $\bar{C}_{\mathcal{O}}$ in (14) and the usual $\delta V_L$, $V_R$, $g_L$, and $g_R$ $tbW$ form factors is

$$\begin{aligned}
V_L &= V_{tb} + y_t^2 \bar{C}^{(-)33}_{\varphi q}, \qquad V_R = y_t^2 \frac{1}{2}\bar{C}^{33}_{\varphi ud}, \\
g_L &= -y_t g\sqrt{2}\bar{C}^{33}_{dW}, \qquad g_R = -y_t g\sqrt{2}\bar{C}^{33}_{uW}.
\end{aligned} \tag{16}$$

There have been many studies that have set bounds on the coefficients of these operators based mostly on LHC ($\sqrt{s} = 7$, 8 TeV) single-top production and $W$-helicity fractions in top decay [24,35–40]. A recent LHC combined extraction of $|f_{LV}V_{tb}|$ has been presented at $1\sigma$ level [35]

$$|f_{LV}V_{tb}| = 1.02 \pm 0.08(\text{meas}) \pm 0.04(\text{theo}), \tag{17}$$

where $f_{LV}V_{tb} \equiv V_L$ in our notation. From this, we can set $-0.16 < \bar{C}^{(-)33}_{\varphi q} < 0.20$ at $2\sigma$ (or 95%) level, if we assume $V_{tb} = 1$. Concerning the other couplings, with the constraint $V_L = 1$, CMS has reported a global analysis based on two- and three-dimensional fit scenarios, from which they have obtained the most stringent 95% C.L. bounds to date [24]

$$|V_R| < 0.16, \quad |g_L| < 0.057, \quad -0.049 < g_R < 0.048. \tag{18}$$

These limits can be converted to bounds on the effective couplings $\bar{C}_{\mathcal{O}}$ through (16),

$$\begin{aligned}
&-0.16 < \bar{C}^{(-)33}_{\varphi q} < 0.20, \qquad |\bar{C}^{33}_{\varphi ud}| < 0.32, \\
&-0.053 < \bar{C}^{33}_{uW} < 0.052, \qquad |\bar{C}^{33}_{dW}| < 0.062,
\end{aligned} \tag{19}$$

which are therefore the current LHC bounds on the effective dimension 6 couplings $\bar{C}_{\mathcal{O}}$.

What could be the improvement of these limits in the LHC top physics program, assuming no beyond the SM physics is found? With integrated luminosities of up to 20 $\text{fb}^{-1}$ already obtained, the statistical uncertainties are subdominant relative to the systematic and other uncertainties. We could then expect that even the High-Luminosity LHC (HL-LHC) phase will not necessarily yield an order-of-magnitude improvement over the limits (18) and (19). For instance, in [23], the 95% C.L. limits $|\bar{C}_{\varphi q}^{(-)33}| < 0.5$ and $|\bar{C}_{uW}^{33}| < 0.25$ are obtained based on CMS and ATLAS $ttZ$ cross section measurements. A projection is then made in [23] for as much as 3 $\text{ab}^{-1}$ of pseudodata leading to the estimates $|\bar{C}_{\varphi q}^{(-)33}| < 0.2$ and $|\bar{C}_{uW}^{33}| < 0.15$, which amount to an improvement by a factor of 2.

The ILC $t\bar{t}$ production process has the potential of improving the $\bar{C}_{\varphi q}^{(-)33}$ and $\bar{C}_{uW}^{33}$ bounds by an order of magnitude or more [22,23,41]. Specifically, as reported in [22], the ILC at $\sqrt{s} = 500$ GeV based on $t\bar{t}$ cross section and forward-backward (FB) asymmetry measurements, and assuming an experimental uncertainty of 5% in the cross section and 2% in the FB asymmetry, would give the single-coupling bounds

$$|\bar{C}_{\varphi q}^{(-)33}| < 0.04, \qquad |\bar{C}_{uW}^{33}| < 0.006. \tag{20}$$

In [23], for the same energy, an experimental uncertainty of 1% is assumed, which yields correspondingly tighter individual-coupling direct bounds

$$|\bar{C}_{\varphi q}^{(-)33}| < 0.015, \qquad |\bar{C}_{uW}^{33}| < 0.0011, \tag{21}$$

as shown in Fig. 6 of that reference. Notice that (21) assumes also longitudinal beam polarizations $(\mathcal{P}_{e^-}, \mathcal{P}_{e^+}) = (-80\%, +30\%)$ [23]. Bear in mind that there are another two operators with $ttZ$ couplings that also contribute to $t\bar{t}$ production. When the simultaneous contributions of these operators are considered, the marginalized limits are relaxed. This is indeed so with the marginalized limits from the multivariate analysis carried out in [23], which are reported there to be larger than the individual ones (21) by a factor of 17. For the purposes of the present study, however, we take the single-coupling bounds (21) and (20) as benchmarks of the projected sensitivity of $t\bar{t}$ production at the ILC.

### B. Diagonal four-fermion operators

The use of effective Lagrangians in the top quark physics program aims ultimately to constrain simultaneously all the nonredundant operators (at a certain level, like dimension 6) based on all the available experimental measurements. For instance, a recent global fit has been presented in [38] where four top-gauge boson and five four-fermion operator coefficients were constrained using both $t\bar{t}$ as well as single-top production measurements from the LHC and the Tevatron. Not surprisingly, the bounds obtained by considering effects from one operator at a time tend to greatly relax when other operators are also taken into account [38]. There is indeed a great effort to perform global fit studies, as is found in the literature [37]. Besides the motivation for making an analysis complete, the goal of considering all the operators is for consistency. Top-gauge boson operators with derivatives on fermion fields [42] do not appear in the basis of [8] because equations of motion relate them to the ones considered here. These equations involve four-fermion terms that are part of the nonredundant operators. For instance, a $tbW$ coupling is generated by an operator $O_{qW} = \bar{q}_L \gamma^\mu \tau^I D^\nu q_L W^I_{\mu\nu}$ that should be considered in a CC interaction of the top quark. Bearing in mind the general $tbW$ vertex generated by the operators in (15), we can in fact isolate the nonredundant contribution by this operator [29]. However, it is convenient to implement this effect with the four-fermion operator $O_{lq}^{(3)}$ that generates a $\bar{e}_L \gamma^\mu \nu_L \bar{t}_L \gamma_\mu b_L$ interaction instead [29],

$$O_{qW}^{33} + (O_{qW}^{33})^\dagger = \frac{g}{2}(O_{\varphi q}^{(3)33} + (O_{\varphi q}^{(3)33})^\dagger) + \frac{g}{2}\sum_{k=1}^{3}(O_{\ell q}^{(3)kk33} + O_{qq}^{(3)kk33}). \tag{22}$$

In this sense, an analysis of top-gauge boson couplings should be considered complete and consistent only if it includes four-fermion operators.

There are eight diagonal four-fermion operators involving two first-generation leptons and two third-generation quarks. Four of them are associated with CC couplings and the other four to only NC couplings. The CC operators that contribute to single-top production are

$$\begin{aligned} O_{\ell q}^{(3)13} &= \bar{\ell}\gamma_\mu \tau^I \ell \bar{q}\gamma^\mu \tau^I q \\ &= 2(\bar{\nu}_L \gamma_\mu e_L \bar{b}_L \gamma^\mu t_L + \bar{e}_L \gamma_\mu \nu_L \bar{t}_L \gamma^\mu b_L) \\ &\quad + (\bar{\nu}_L \gamma_\mu \nu_L - \bar{e}_L \gamma_\mu e_L)(\bar{t}_L \gamma_\mu t_L - \bar{b}_L \gamma_\mu b_L) \\ O_{\ell edq}^{13} &= \bar{\nu}_L e_R \bar{b}_R t_L + \bar{e}_L e_R \bar{b}_R b_L \\ O_{\ell equ}^{(1)13} &= \bar{\nu}_L e_R \bar{b}_L t_R - \bar{e}_L e_R \bar{t}_L t_R \\ O_{\ell equ}^{(3)13} &= \bar{\nu}_L \sigma^{\mu\nu} e_R \bar{b}_L \sigma_{\mu\nu} t_R - \bar{e}_L \sigma^{\mu\nu} e_R \bar{t}_L \sigma_{\mu\nu} t_R, \end{aligned} \tag{23}$$

where we have used the abbreviated notation $O^{13}$ for $O^{1133}$.

To date, there are no reported limits based on LHC nor Fermilab top production and/or decay processes for these operators. In [11], it has been pointed out that distribution-based measurements like the $W$-helicity fractions could in

principle be used to this end as the leptonic decay is used to analyze the $W$ polarization. However, the experimental requirement that $m_{\ell\nu}$ be close to $M_W$ severely reduces the sensitivity of the fractions to the four-fermion operators [11].

## IV. EFFECTIVE COUPLINGS IN SINGLE-TOP PRODUCTION AND DECAY

For the computation of the cross section with anomalous effective vertices, we use MG5, as described in Sec. II B. For computational purposes, we set the scale $\Lambda = 10$ TeV in (13) and (14). The effective operators (15) and (23) were implemented in MG5 by means of the program FeynRules version 2.0 [43].

The Feynman diagrams for the processes (2) containing effective vertices are illustrated in Figs. 9–13. As discussed in Sec. II A, there are 116 diagrams for semileptonic single-top production and decay in the SM with Cabibbo mixing, in the $e^-\bar{\nu}_e$ channel. When the effective operators are switched on in Lagrangian (13), there are 296 additional diagrams with one vertex from the operators (15) and none from the operators (23), or $N_{tbW} = 1$, $N_{4f} = 0$; 220 with $N_{tbW} = 2$, $N_{4f} = 0$; 40 with $N_{tbW} = 3$, $N_{4f} = 0$; 124 with $N_{tbW} = 0$, $N_{4f} = 1$; 24 with $N_{tbW} = 0$, $N_{4f} = 2$; 192 with $N_{tbW} = 1$, $N_{4f} = 1$; 20 with $N_{tbW} = 1$, $N_{4f} = 2$; and 60 with $N_{tbW} = 2$, $N_{4f} = 1$, for a total of 976 additional diagrams.

Diagrams with one, two, and three effective vertices entering the amplitude for (2), contribute to it at $\mathcal{O}(\Lambda^{-n})$ with $n = 2$, 4, and 6, respectively. In fact, once the top propagator dependence on effective couplings through the top decay width is taken into account, the scattering amplitude is given as a power series of $\Lambda^{-2}$. We remark that diagrams with two effective vertices must be kept in the amplitude, since, through their interference with SM diagrams, they make contributions to the cross section of the same order $\mathcal{O}(\Lambda^{-4})$ as the square of diagrams with only

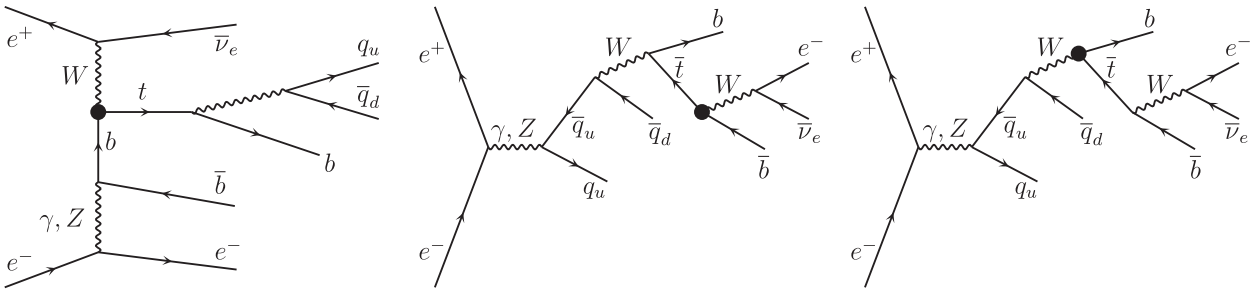


FIG. 9. Sample Feynman diagrams with one anomalous three-particle vertex from the operators (15).

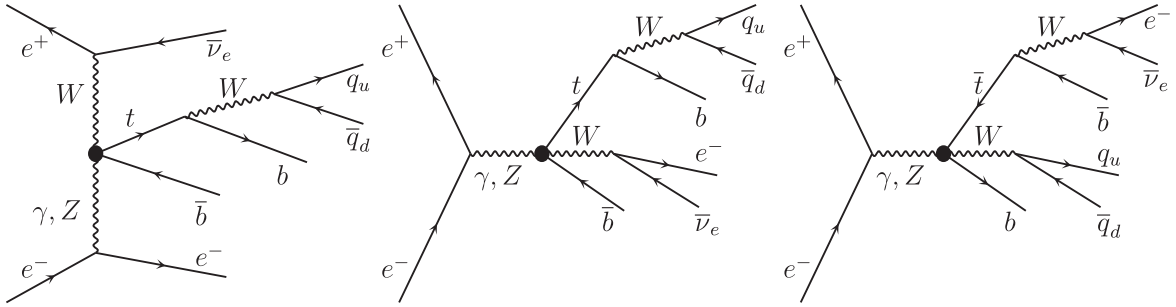


FIG. 10. All Feynman diagrams with one anomalous four-particle vertex from the operators $O_{uW}^{33}$, $O_{dW}^{33}$ in (15).

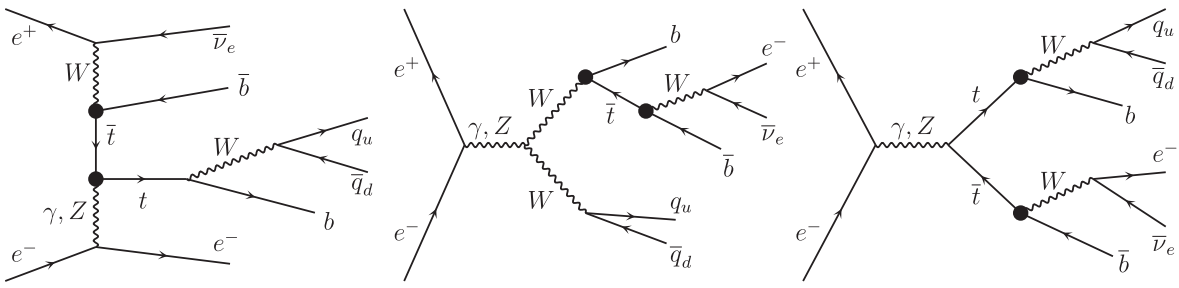


FIG. 11. Sample Feynman diagrams with two and three anomalous vertices from the operators (15).

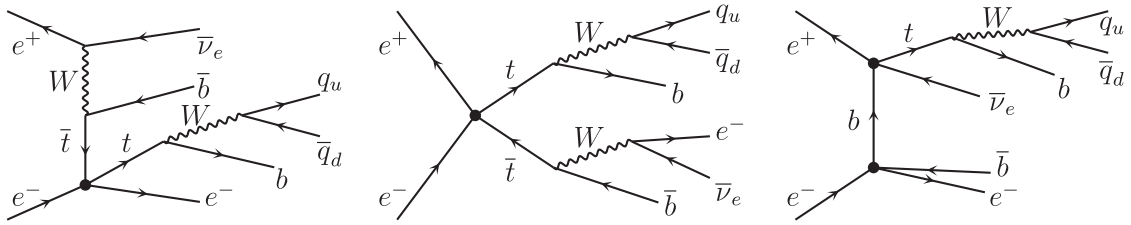


FIG. 12. Sample Feynman diagrams with one and two four-fermion vertices from the operators (23).

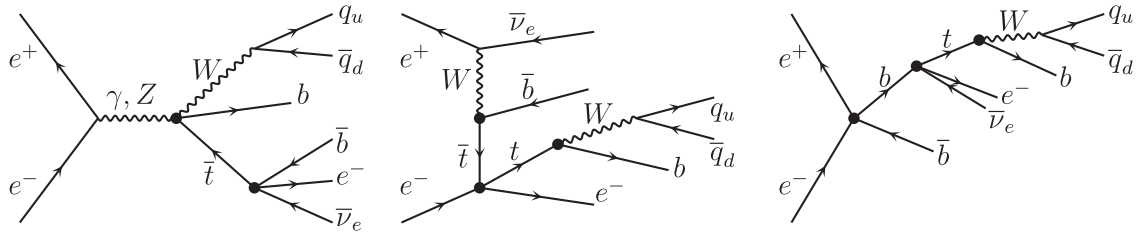


FIG. 13. Sample Feynman diagrams with both gauge-boson and four-fermion vertices from the operators (15) and (23).

one effective vertex. We have actually taken into account the contributions from diagrams with three effective vertices in our calculation, as well as the dependence of the top decay width on the effective couplings, but we have explicitly verified in all cases that the contribution to the cross section from terms of order higher than $\mathcal{O}(\Lambda^{-4})$ is actually negligible for values of the effective couplings within the bounds given below. (We remark here, parenthetically, that the contributions to the cross section at order $1/\Lambda^4$ from dimension 8 operators interfering with the SM are currently unknown and constitute an inherent uncertainty of the effective field-theory analysis at dimension 6.)

### A. Methodology and assumptions

In order to obtain bounds on the effective couplings, we consider the ratio of the cross section $\sigma_{\text{eff}}(\{\bar{C}_{\mathcal{O}}\})$ obtained from the Lagrangian (13) at tree level to the SM cross section $\sigma_{\text{SM}} = \sigma_{\text{eff}}(\{0\})$

$$R = \frac{\sigma_{\text{eff}}(\{\bar{C}_{\mathcal{O}}\})}{\sigma_{\text{SM}}}, \tag{24}$$

where $\{\bar{C}_{\mathcal{O}}\}$ is the set of anomalous coupling constants. For a given relative experimental uncertainty $\varepsilon_{\text{expt}}$., the region of allowed values for the effective couplings $\{\bar{C}_{\mathcal{O}}\}$ is determined at the $1\sigma$ level by the inequalities

$$R \lesseqgtr 1 \pm \varepsilon_{\text{expt}}. \tag{25}$$

We obtain allowed intervals on the effective couplings taken to be nonzero one at a time by parametrizing the ratio (24) as

$$R = 1 + a\bar{C}_{\mathcal{O}} + b\bar{C}_{\mathcal{O}}^2 + \cdots, \tag{26}$$

where the ellipsis refers to higher powers of $\bar{C}_{\mathcal{O}}$. Similarly, we consider also allowed two-coupling regions for pairs of effective couplings by parametrizing (24) as

$$R = 1 + a\bar{C}_{\mathcal{O}} + b\bar{C}_{\mathcal{O}}^2 + a'\bar{C}_{\mathcal{O}'} + b'\bar{C}_{\mathcal{O}'}^2 + c\bar{C}_{\mathcal{O}}\bar{C}_{\mathcal{O}'} + \cdots, \tag{27}$$

with $\bar{C}_{\mathcal{O}}$ and $\bar{C}_{\mathcal{O}'}$ the effective couplings under consideration, and all other ones set to zero. The parameters in (26) and (27) are determined from an extensive set of MG5 simulations to which (26) and (27) are fitted. Once those parameters are known, (25) yields the desired one- or two-dimensional limits on the effective couplings being considered. The consistency condition that the contribution to the cross section from terms of $\mathcal{O}(\Lambda^{-6})$ and higher in (13) be negligibly small entails on the parametrizations (26) and (27) the requirement that the terms of $\mathcal{O}(\bar{C}^3)$ and higher must be correspondingly negligible within the allowed region determined by (25). We check this consistency condition in all cases considered below.

In order to obtain bounds on the effective couplings through (25), below we assume $\varepsilon_{\text{expt}}$. to take values within certain intervals. We motivate those assumed ranges for $\varepsilon_{\text{expt}}$. by estimating the uncertainties in the signal cross section in our Monte Carlo simulations, through the addition in quadrature of the statistical uncertainty and the irreducible background given at the end of Sec. II B and the uncertainties arising from the $t\bar{t}$ background as discussed in Sec. II C. This leads us to assume that, at $\sqrt{s} = 3$ TeV, $\varepsilon_{\text{expt}}$. is in the range 5%–9% and at $\sqrt{s} =$ 1 TeV within 5%–15%. In the case of $\sqrt{s} = 0.5$ TeV, we assume $\varepsilon_{\text{expt}}$. to lie in the interval 10%–20%, but present also some results at 30%. As discussed in more detail below, at all three energies, the individual-coupling limits

we obtain can be extrapolated to values of $\varepsilon_{\text{expt}}$. moderately lower or higher than the ranges we assume. Furthermore, as discussed in Sec. II E, beam polarization may contribute to reduce background uncertainties, which may help reach the lower end of the assumed uncertainty intervals, especially at $\sqrt{s} = 0.5$ TeV.

### B. Results

The single-coupling bounds obtained from (25) are reported in Table V for effective $tbW$ couplings and Table VI for effective four-fermion couplings. The validity of the quadratic dependence (26) of the cross section on the effective couplings is verified to hold for all couplings at the three energies and three experimental uncertainties shown in the tables, with one exception. The lower bound for $\bar{C}_{\varphi q}^{(-)33}$ at $\sqrt{s} = 3$ TeV at the highest value of $\varepsilon_{\text{expt}}$. lies outside the interval of validity of the quadratic approximation (26), which we estimate to be $-0.12 < \bar{C}_{\varphi q}^{(-)33} < 0.12$ at that energy. That value is therefore omitted from Table V. There is, however, no loss of relevant information in that omission, since we see from Table V that the cross section at ILC energies is more sensitive than at CLIC to $\bar{C}_{\varphi q}^{(-)33}$.

When the interference of diagrams containing one effective vertex from the operator $\mathcal{O}$ with those from the SM vanishes, or is suppressed by a small mass parameter, the linear term in (24) is suppressed and the bounds on $\bar{C}_{\mathcal{O}}$ are symmetric about the origin. This is the case, in particular, for the couplings $\bar{C}_{\mathcal{O}i}$ associated with the anti-Hermitian part of $\mathcal{O}$, $i/2(\mathcal{O} - \mathcal{O}^\dagger)$, since those operators are $CP$ odd and cannot interfere with the SM operators which are $CP$ even. (Notice that we are only taking into account Cabibbo mixing in this paper, so that all of the parameters in the SM charged current are real.) On the other hand, when the interference of diagrams with a vertex from the Hermitian part of $\mathcal{O}$ with the SM is suppressed, the bounds on $\bar{C}_{\mathcal{O}r}$ and $\bar{C}_{\mathcal{O}i}$ are the same and are denoted $\bar{C}_{\mathcal{O}r|i}$ in Table V and $\bar{F}_{\mathcal{O}r|i}$ in Table VI.

At $\sqrt{s} = 0.5$, for an experimental uncertainty $\varepsilon_{\text{expt}} = 30\%$, we obtain the individual-coupling limits

$$\begin{aligned} &-0.14 < \bar{C}_{\varphi q}^{(-)33} < 0.13, \qquad -1.42 < \bar{C}_{\varphi udr|i}^{33} < 1.37, \\ &|\bar{C}_{\varphi udi}^{33}| < 1.40, \qquad -0.055 < \bar{C}_{uWr}^{33} < 0.049, \\ &|\bar{C}_{uWi}^{33}| < 0.19, \qquad -0.25 < \bar{C}_{dWr}^{33} < 0.22, \\ &|\bar{C}_{dWi}^{33}| < 0.23. \end{aligned} \tag{28}$$

TABLE V. Single-coupling limits on effective $tbW$ couplings, for three values of $\sqrt{s}$ and three assumed experimental uncertainties.

| $\sqrt{s}$ (TeV) | 0.5 | | | 1 | | | 3 | | |
|---|---|---|---|---|---|---|---|---|---|
| $\varepsilon_{\text{expt}}$ (%) | 10 | 15 | 20 | 5 | 10 | 15 | 5 | 7 | 9 |
| $\bar{C}_{fq}^{(-)33}$ | −0.033<br>0.056 | −0.057<br>0.076 | −0.083<br>0.095 | −0.031<br>0.015 | −0.056<br>0.036 | −0.082<br>0.057 | −0.030<br>0.054 | −0.067<br>0.066 | ⋯<br>0.077 |
| $\bar{C}_{fudr}^{33}$ | −0.90<br>0.85 | −1.05<br>1.00 | −1.19<br>1.14 | −0.32<br>0.31 | −0.50<br>0.49 | −0.63<br>0.62 | −0.21<br>0.20 | −0.24<br>0.23 | −0.26<br>0.25 |
| $\bar{C}_{fudi}^{33}$ | ±0.87 | ±1.03 | ±1.16 | ±0.31 | ±0.50 | ±0.63 | ±0.21 | ±0.24 | ±0.26 |
| $\bar{C}_{uWr}^{33}$ | −0.013<br>0.021 | −0.022<br>0.028 | −0.032<br>0.035 | −0.013<br>0.0058 | −0.025<br>0.014 | −0.041<br>0.021 | −0.046<br>0.020 | −0.050<br>0.023 | −0.053<br>0.027 |
| $\bar{C}_{uWi}^{33}$ | ±0.12 | ± 0.14 | ±0.15 | ±0.030 | ±0.050 | ±0.060 | ±0.030 | ±0.034 | ±0.038 |
| $\bar{C}_{dWr}^{33}$ | −0.16<br>0.13 | −0.19<br>0.16 | −0.21<br>0.18 | −0.033<br>0.028 | −0.050<br>0.046 | −0.063<br>0.058 | −0.025<br>0.025 | −0.029<br>0.029 | −0.032<br>0.032 |
| $\bar{C}_{dWi}^{33}$ | ±0.15 | ±0.17 | ±0.19 | ±0.031 | ±0.048 | ±0.061 | ±0.025 | ±0.029 | ±0.032 |

TABLE VI. Single-coupling bounds on effective four-fermion couplings, for three values of $\sqrt{s}$ and three assumed experimental uncertainties.

| $\sqrt{s}$ (TeV) | 0.5 | | | 1 | | | 3 | | |
|---|---|---|---|---|---|---|---|---|---|
| $\varepsilon_{\text{expt}}$ (%) | 10 | 15 | 20 | 5 | 10 | 15 | 5 | 7 | 9 |
| $\bar{F}_{\ell q}^{(3)13} \times 10^2$ | −0.28<br>0.48 | −0.48<br>0.65 | −0.69<br>0.83 | −0.067<br>0.033 | −0.12<br>0.080 | −0.18<br>0.13 | −0.025<br>0.045 | −0.047<br>0.055 | −0.082<br>0.065 |
| $\bar{F}_{ledqr\|i}^{13} \times 10^2$ | ±5.8 | ±6.9 | ±7.8 | ±0.58 | ±0.92 | ±1.2 | ±0.21 | ±0.24 | ±0.26 |
| $\bar{F}_{\ell equr\|i}^{(1)13} \times 10^2$ | ±2.4 | ±2.8 | ±3.2 | ±0.36 | ±0.56 | ±0.71 | ±0.26 | ±0.30 | ±0.33 |
| $\bar{F}_{\ell equr\|i}^{(3)13} \times 10^2$ | ±0.77 | ±0.91 | ±1.0 | ±0.14 | ±0.21 | ±0.27 | ±0.076 | ±0.086 | ±0.095 |

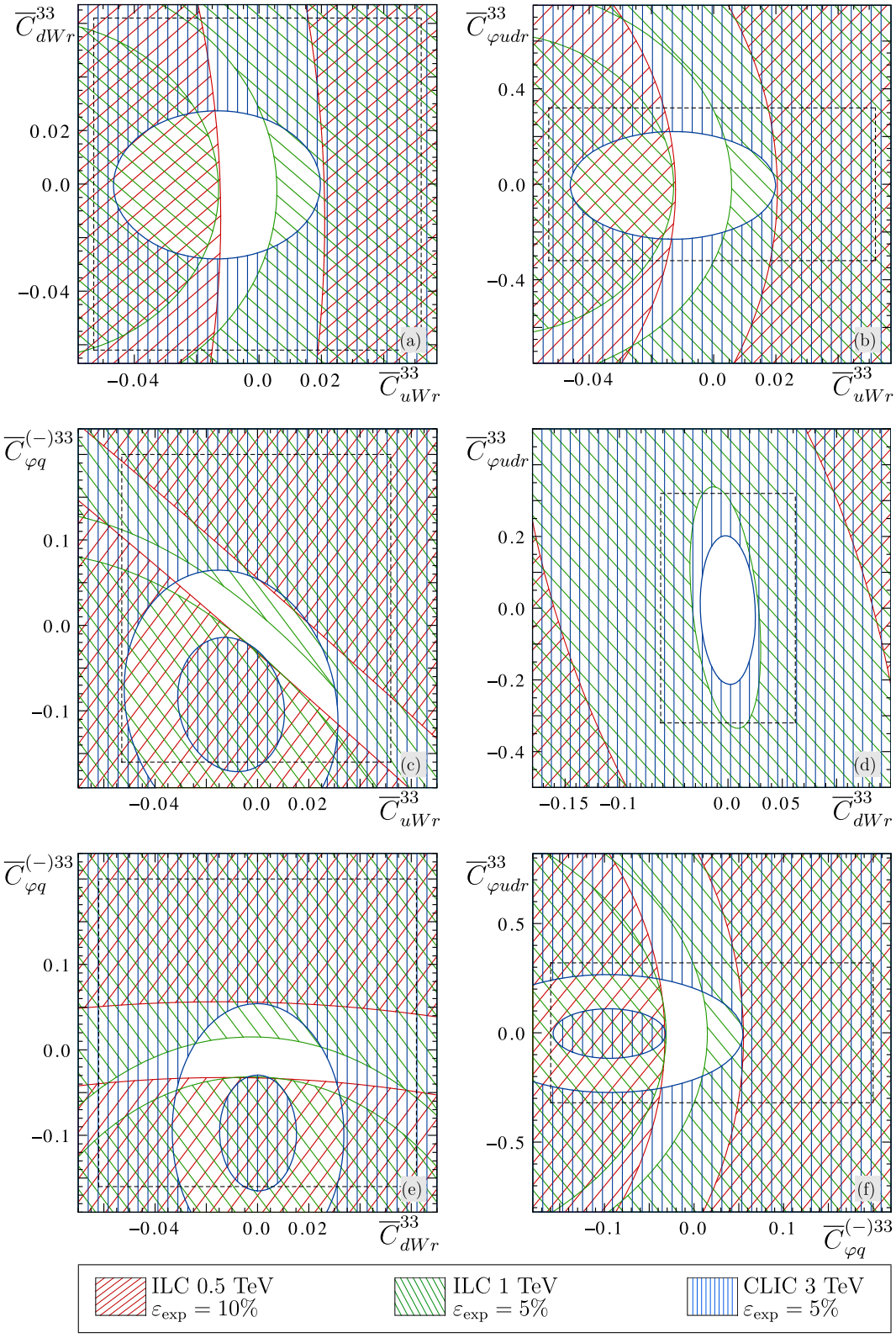


FIG. 14. Parameter regions excluded at 68% C.L. by a measurement of the total cross section for process (2), for the $tbW$ effective coupling pairs (a) $\bar{C}^{33}_{uWr} - \bar{C}^{33}_{dWr}$, (b) $\bar{C}^{33}_{uWr} - \bar{C}_{\varphi udr}$, (c) $\bar{C}^{33}_{\mu Wr} - \bar{C}^{(-)33}_{\varphi q}$, (d) $\bar{C}^{33}_{dWr} - \bar{C}_{\varphi udr}$, (e) $\bar{C}^{33}_{dWr} - \bar{C}^{(-)33}_{\varphi q}$, (f) $\bar{C}^{(-)33}_{\varphi q} - \bar{C}_{\varphi udr}$. (Red hatched areas) $\sqrt{s} = 0.5$ TeV, $\varepsilon_{\text{expt}} = 10\%$. (Green hatched areas) $\sqrt{s} = 1$ TeV, $\varepsilon_{\text{expt}} = 5\%$. (Blue hatched areas) $\sqrt{s} = 3$ TeV, $\varepsilon_{\text{expt}} = 5\%$. (Dashed lines) CMS bounds from (19).

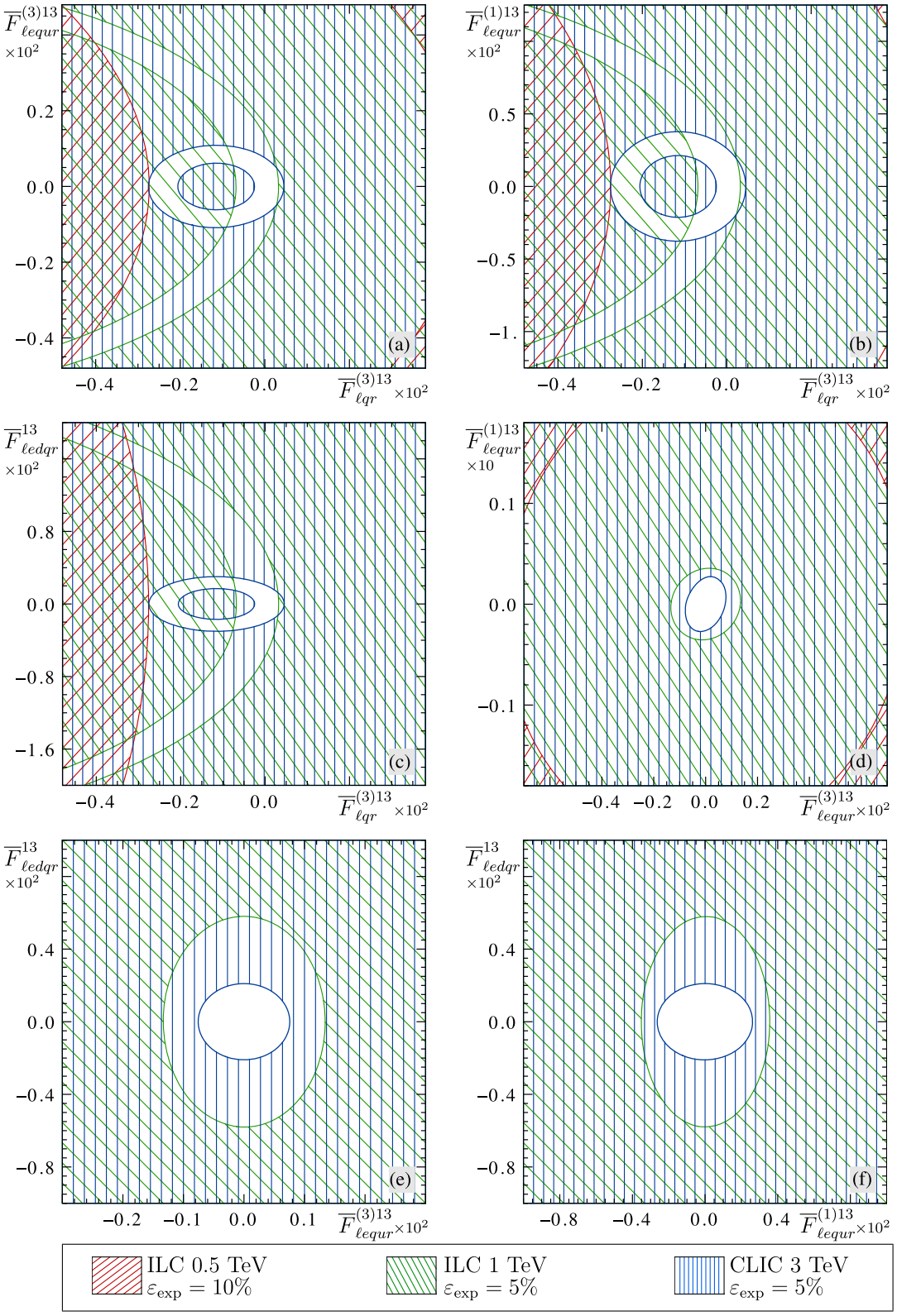


FIG. 15. Parameter regions excluded at 68% C.L. by a measurement of the total cross section for process (2), for the $tbe\nu_e$ four-fermion charged-current coupling pairs (a) $\bar{F}^{(3)13}_{\ell q} - \bar{F}^{(3)13}_{\ell equr}$, (b) $\bar{F}^{(3)13}_{\ell q} - \bar{F}^{(1)13}_{\ell equr}$, (c) $\bar{F}^{(3)13}_{\ell q} - \bar{F}^{13}_{\ell edqr}$, (d) $\bar{F}^{(3)13}_{\ell equr} - \bar{F}^{(1)13}_{\ell equr}$, (e) $\bar{F}^{(3)13}_{\ell equr} - \bar{F}^{13}_{\ell edqr}$, (f) $\bar{F}^{(1)13}_{\ell equr} - \bar{F}^{13}_{\ell edqr}$. Color codes as in the previous figure.

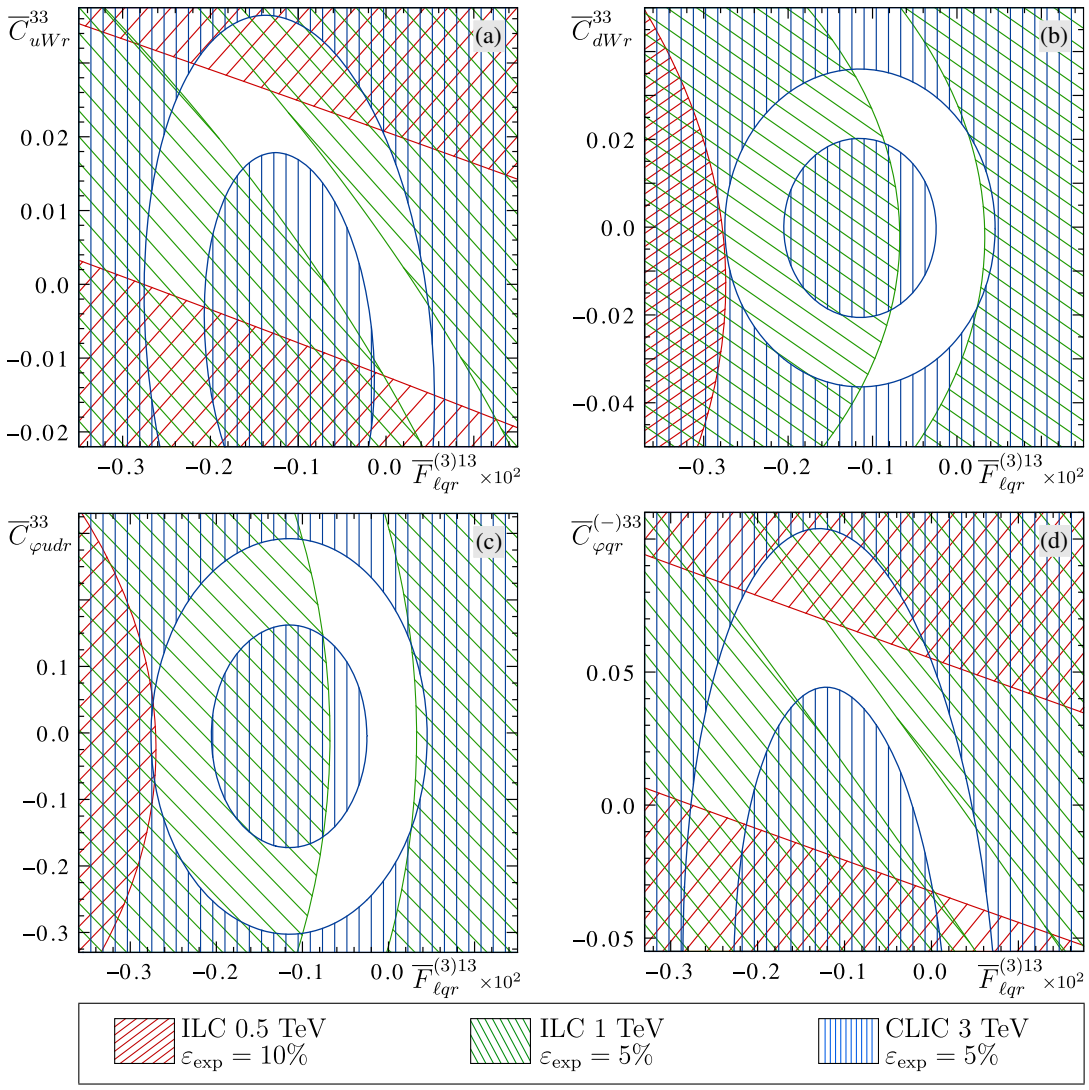


FIG. 16. Parameter regions excluded at 68% C.L. by a measurement of the total cross section for process (2), for the four-fermion coupling $\bar{F}^{(3)13}_{\ell qr}$ together with the $tbW$ effective couplings (a) $\bar{C}^{33}_{uWr}$, (b) $\bar{C}^{33}_{dWr}$, (c) $\bar{C}^{33}_{uWr}$, (d) $\bar{C}^{33}_{\varphi q}$. Color codes as in the previous figure.

At that energy, the signal cross section is most sensitive to $\bar{C}^{(-)33}_{\varphi q}$ and $\bar{C}^{33}_{uWr}$, for which the bounds in (28) are close to the current limits set by CMS, as quoted above in (19). Thus, in order to improve on the current CMS bounds on those couplings, the single-top cross section should be measured by the ILC at $\sqrt{s} = 0.5$ TeV with an uncertainty $\varepsilon_{\rm expt} < 30\%$. We point out also that, at that energy and with an unrealistically low uncertainty $\varepsilon_{\rm expt} = 5\%$, we would obtain the limits $-0.0093 < \bar{C}^{(-)33}_{\varphi q} < 0.035$. Comparison with the bounds at the same uncertainty in Table V leads to the conclusion that the sensitivity to $\bar{C}^{(-)33}_{\varphi q}$ for a fixed relative uncertainty is smaller at CLIC than at the ILC.

The single-coupling bounds in Table VI show both a large sensitivity to $\bar{F}$ couplings relative to that of $\bar{C}$'s, and a strong enhancement of that sensitivity with increasing energy, as expected of four-fermion interactions. As also seen from the table, the single-top cross section is most sensitive to $\bar{F}^{(3)13}_{\ell q}$, which is related to the fact that the operator $O^{(3)13}_{\ell q}$ in (23) is the only four-fermion operator leading to substantial interference with the SM. In the case of $\sqrt{s} = 0.5$ TeV, if we assume an experimental uncertainty $\varepsilon_{\rm expt} = 30\%$, we obtain the bounds

$$-0.011 < \bar{F}^{(3)13}_{\ell q} < 0.012, \qquad |\bar{F}^{13}_{ledqr|i}| < 0.093,$$
$$|\bar{F}^{(1)13}_{\ell equr|i}| < 0.038, \qquad |\bar{F}^{(3)13}_{\ell equr|i}| < 0.012, \tag{29}$$

which still are rather strong.

At each energy, Tables V and VI give lower and upper bounds for each coupling, for three different values of $\varepsilon_{\rm expt}$. As is easy to check, any of those three values results from linear interpolation of the other two, within about 5%. This shows, heuristically, that linear interpolation is valid and can be used to find bounds corresponding to other values of

$\varepsilon_{\text{expt}}$. within the range given in the table. Linear extrapolation can also be used to obtain bounds for $\varepsilon_{\text{expt}}$ moderately smaller than the lowest value used in the table or moderately larger than the highest one. An illustration of this is provided by the bounds at $\sqrt{s} = 0.5$ TeV and $\varepsilon_{\text{expt}} = 30\%$ given above in (28) [respectively, (29)], which agree with an extrapolation from Table V (respectively, Table VI) within at most 5% deviation.

The allowed regions for pairs of effective couplings involving gauge bosons are displayed in Fig. 14, where the current LHC bounds from (19) are also displayed for reference. The allowed regions for pairs of effective four-fermion couplings are displayed in Fig. 15. As can be seen in Figs. 14 and 15, with the exception of the couplings in Figs. 14(d) and 15(d)–15(f), the cross section at the ILC at either $\sqrt{s} = 0.5$ or 1 TeV does not determine a small, simply connected neighborhood of the origin, but rather an extended toroidal band. However, the intersection of those two regions does provide a simply connected vicinity of the SM. Those ILC-allowed regions are further constrained by the bounds imposed by CLIC, as shown in the figures.

The term containing the coefficient $c$ in (27), corresponding to the interference of two anomalous amplitudes, leads to a rotation of the symmetry axes of the allowed region relative to the coordinate axes. Interference effects between the amplitudes proportional to $C^{33}_{\varphi udr}$ and $C^{33}_{dWr}$ are apparent in Fig. 14(d), sizable at $\sqrt{s} = 0.5$ TeV and significantly weaker at higher energies. Smaller, but still noticeable interference between amplitudes proportional to $\bar{C}^{(-)33}_{\varphi q}$ and $\bar{C}^{33}_{uWr}$ is seen in Fig. 14(c). All other pairs of couplings correspond to effective operators involving $b$-quark fields of opposite chiralities, for which interference is suppressed by the small $b$-quark mass. On the other hand, no interference effects are visible in Fig. 15, except for a weak one in panel (c) at the lowest $\sqrt{s}$. In particular, the regions allowed by the single-top cross section at $\sqrt{s} = 0.5$ TeV not shown in Figs. 15(e) and 15(f) are ellipses with their axes parallel to the coordinate axes, inscribed within the rectangles defined by the single-coupling bounds in Table VI.

As discussed in Sec. III B, the operator $O^{(3)13}_{lq}$ is related to certain gauge-boson operators by the equations of motion. In Fig. 16, we show the allowed regions for pairs of couplings involving $\bar{F}^{(3)13}_{\ell qr}$ and one gauge-boson effective coupling.

## V. FINAL REMARKS

Top quark physics is an essential part of the future ILC and CLIC collider programs. While so far most of the interest has focused on $t\bar{t}$ production and its great sensitivity to NC $ttZ(A)$ couplings, in this paper, we discuss whether the single-top mode would provide any useful information. In this context, it is important to stress the fact that, while at the ILC, single-top is subdominant to top-pair production, which then becomes a strong background, at CLIC, single top is the dominant top production mode. We have carried out a preliminary parton level analysis of the semileptonic six-fermion final state $b\bar{b}e^-\nu_e q_u q_d$ (and its charge conjugate) in the context of single-top production and have found that, at the three energies considered, $\sqrt{s} = 0.5$, 1, and 3 TeV, the signal cross sections are about 1–2 fb (see Table III), including phase-space cuts and $b$-tagging efficiencies, enough to keep the statistical uncertainties under 5%. A detailed discussion of backgrounds is given in Sec. II.

We have obtained individual limits on $tbW$ vertices in the context of the $\mathrm{SU}(2) \times \mathrm{U}(1)$-gauge-invariant effective dimension 6 operators [8], as shown in Table V and Fig. 14. In order to discuss our results for the four top-gauge boson couplings generating CC vertices, it is convenient to separate them in two pairs. In the first pair, we have the operators $O^{(-)33}_{\varphi q}$ and $O^{33}_{uW}$, which have in common that they both generate interference with the SM, simultaneously generate an additional NC $ttZ/A$ coupling, and contribute substantially to $s$-channel diagrams that appear in both single-top and top-pair production. With increasing energy, both the effects of interference and the $s$-channel contribution decrease and so does the sensitivity to these couplings. To compare our results to those from the LHC given in (19) and to the projections for $t\bar{t}$ production at the ILC, (20) and (21), we take the inverse of the length of the interval determined by the single-coupling bounds in those equations and in Table V as a measure of the sensitivity. For the coupling $\bar{C}^{(-)33}_{\varphi q}$, the sensitivity obtained at $\sqrt{s} = 0.5$ TeV if we assume an experimental uncertainty of 10% is 4 times larger than at the LHC, (19), and about the same as that of $t\bar{t}$ production at the same energy, with the experimental uncertainties for $t\bar{t}$ assumed in (20), but three times smaller if the uncertainties are those assumed in (21). Larger assumed experimental uncertainties lead, of course, to correspondingly smaller sensitivities. As discussed in relation to (28), for an experimental uncertainty of about 30%, the sensitivity to $\bar{C}^{(-)33}_{\varphi q}$ at $\sqrt{s} = 0.5$ TeV becomes equal to the current LHC result. As seen from Table V, the largest sensitivity to $\bar{C}^{(-)33}_{\varphi q}$ is obtained at $\sqrt{s} = 1$ TeV if we assume an experimental uncertainty of 5%. In that case, the sensitivity is about 8 times larger than the current LHC result, almost twice as large as the ILC $t\bar{t}$ sensitivity in (20) and slightly smaller than in (21). Thus, for the coupling $\bar{C}^{(-)33}_{\varphi q}$, we expect the sensitivity of single-top production at linear $e^-e^+$ colliders to significantly improve the current one at the LHC and the projected one at the HL-LHC and to be competitive with the sensitivity of $t\bar{t}$ production at the ILC.

For the coupling $\bar{C}^{33}_{uWr}$, at $\sqrt{s} = 0.5$ TeV and with an experimental uncertainty of 10%, the sensitivity from

Table V is 3 times larger than that from the current LHC result (19), though almost 3 times smaller than the ILC $t\bar{t}$ production result (20), and about 15 times smaller than (21). The largest sensitivity to this coupling in Table V occurs at $\sqrt{s} = 1$ TeV for an assumed experimental uncertainty of 5%, which is 5 times larger than the current LHC result (19), slightly smaller than the ILC $t\bar{t}$ sensitivity (20), and an order of magnitude smaller than (21). In this case, we conclude that the sensitivity to $\bar{C}^{33}_{uWr}$ of single-top production at the ILC will improve on the current LHC sensitivity by a factor of 3–5, but will be significantly worse than that of $t\bar{t}$ production at the ILC.

The operators $O^{33}_{\varphi ud}$ and $O^{33}_{dW}$ do not appreciably contribute to $t\bar{t}$ production at the ILC, and lead to very modest interference with the SM amplitudes. They contribute to single-top production in $e^-e^+$ collisions mostly through $t$-channel diagrams, with the contribution from $s$-channel diagrams remaining essentially a SM input that is important at lower energies but becomes very small for energies higher than $\sqrt{s} = 2$ TeV. In this respect, we notice that $O^{33}_{\varphi ud}$ does not generate NC interactions and that $O^{33}_{dW}$ only generates, besides $tbW$, a $bbZ$ coupling with very little effect on $s$-channel diagrams. As a result, the sensitivity to these operators increases with energy.

The sensitivity to $\bar{C}^{33}_{\varphi udr}$ at $\sqrt{s} = 0.5$ TeV with an assumed experimental uncertainty of 10%, as given in Table V, is less than half that of the current LHC limits (19). At $\sqrt{s} = 1$ TeV with an assumed uncertainty of 5% is equal to the sensitivity of the current LHC results (19) and at $\sqrt{s} = 3$ TeV with uncertainty 5% is about 60% larger than the current LHC sensitivity. For this coupling, therefore, at most a slight improvement over the current LHC sensitivity can be expected from CLIC and none from the ILC.

The sensitivity to $\bar{C}^{33}_{dWr}$ at $\sqrt{s} = 0.5$ TeV with an assumed experimental uncertainty of 10%, as given in Table V, is about half that of the current LHC limits (19). At $\sqrt{s} = 1$ TeV with an assumed uncertainty of 5%, it is twice as large as the current LHC sensitivity and 2.5 times as large at $\sqrt{s} = 3$ TeV with uncertainty 5%. Thus, the sensitivity to $\bar{C}^{33}_{dWr}$ at the highest energy $e^-e^+$ collisions increases by a factor of 2–2.5 with respect to the current LHC sensitivity.

These conclusions depend, of course, on the fact that, at each one of the three energies discussed here, we have assumed the lowest experimental uncertainties considered in Table V. With the information contained in that table, however, these conclusions can be adapted to other experimental uncertainty assumptions.

Limits on the four-fermion operators from (23) are given in Table VI and in Figs. 15 and 16. Those CC four-fermion couplings cannot be observed at hadron colliders or in NC processes such as $t\bar{t}$ production at $e^-e^+$ colliders. Therefore, single-top production at those colliders is the only possibility to bound them. Since the sensitivity to four-fermion interactions increases very rapidly with energy, for these couplings, CLIC is clearly the best option. The sensitivity at the 1 TeV ILC is still substantial, however, being about half that for CLIC, as shown in Table VI.

## ACKNOWLEDGMENTS

We gratefully acknowlegde support from Conacyt of México through Research Project 220066 and from Sistema Nacional de Investigadores de México.

[1] T. Behnke *et al.*, arXiv:1306.6327.
[2] H. Baer *et al.*, arXiv:1306.6352.
[3] C. Adolphsen *et al.*, arXiv:1306.6353.
[4] C. Adolphsen *et al.*, arXiv:1306.6328.
[5] T. Behnke *et al.*, arXiv:1306.6329.
[6] L. Linssen *et al.*, arXiv:1202.5940.
[7] P. Lebrun *et al.*, arXiv:1209.2543.
[8] B. Grzadkowski, M. Iskrzyński, M. Misiak, and J. Rosiek, J. High Energy Phys. 10 (2010) 085.
[9] U. Husemann, Prog. Part. Nucl. Phys. **95**, 48 (2017); F. P. Schilling, Int. J. Mod. Phys. A **27**, 1230016 (2012); W. Bernreuther and P. Uwer, Nucl. Part. Phys. Proc. **261–262**, 414 (2015); W. Bernreuther, J. Phys. G **35**, 083001 (2008); Nuovo Cimento Soc. Ital. Fis. **033C**, 3 (2010).
[10] J. de Blas, M. Chala, and J. Santiago, J. High Energy Phys. 09 (2015) 189.
[11] C. Zhang, Phys. Rev. D **90**, 014008 (2014).
[12] S. Willenbrock and C. Zhang, Annu. Rev. Nucl. Part. Sci. **64**, 83 (2014); C. Zhang, N. Greiner, and S. Willenbrock, Phys. Rev. D **86**, 014024 (2012); A. Cordero-Cid, J. M. Hernandez, G. Tavares-Velasco, and J. J. Toscano, J. Phys. G **35**, 025004 (2008); A. Avilez-Lopez, H. Novales-Sanchez, G. Tavares-Velasco, and J. J. Toscano, Phys. Lett. B **653**, 241 (2007); R. Martinez and G. Valencia, Phys. Rev. D **95**, 035041 (2017).
[13] G. Durieux, F. Maltoni, and C. Zhang, Phys. Rev. D **91**, 074017 (2015).
[14] R. A. Coimbra, P. M. Ferreira, R. B. Guedes, O. Oliveira, A. Onofre, R. Santos, and M. Won, Phys. Rev. D **79**, 014006 (2009).
[15] N. Zhou, D. Whiteson, and T. M. P. Tait, Phys. Rev. D **85**, 091501 (2012); E. Alvarez, D. A. Faroughy, J. F. Kamenik, R. Morales, and A. Szynkman, Nucl. Phys. **B915**, 19 (2017); C. Zhang, arXiv:1708.05928; R. Frederix, D. Pagani, and M. Zaro, arXiv:1711.02116.

[16] E. Devetak, A. Nomerotski, and M. Peskin, Phys. Rev. D **84**, 034029 (2011); R. Rntsch and M. Schulze, J. High Energy Phys. 08 (2015) 044; J. Gao and H. X. Zhu, Phys. Rev. Lett. **113**, 262001 (2014); Phys. Rev. D **90**, 114022 (2014); B. C. Nejad, W. Kilian, J. M. Lindert, S. Pozzorini, J. Reuter, and C. Weiss, J. High Energy Phys. 12 (2016) 075; F. Larios, T. M. P. Tait, and C. P. Yuan, Phys. Rev. D **57**, 3106 (1998); G. J. Gounaris and F. M. Renard, Phys. Rev. D **94**, 053009 (2016); W. Bernreuther and L. Chen, Phys. Rev. D **93**, 053018 (2016); N. Bouayed and F. Boudjema, Phys. Rev. D **77**, 013004 (2008); S. Kanemura, D. Nomura, and K. Tsumura, Phys. Rev. D **74**, 076007 (2006); S. Godfrey and S. h. Zhu, Phys. Rev. D **72**, 074011 (2005); T. Han, Y. J. Kim, A. Likhoded, and G. Valencia, Nucl. Phys. **B593**, 415 (2001); A. A. Billur, M. Köksal, and A. Gutiérrez-Rodríguez, Phys. Rev. D **96**, 056007 (2017); Adv. High Energy Phys. **2017**, 6738409 (2017); W. Bernreuther, L. Chen, I. García, M. Perelló, R. P. F. Richard, E. Ros, and M. Vos, arXiv:1710.06737.P. S. Bhupal Dev *et al.*, Phys. Rev. Lett. **100**, 051801 (2008);
[17] E. Boos, Y. Kurihara, M. Sachwitz, H. J. Schreiber, S. Shichanin, and Y. Shimizu, Z. Phys. C **70**, 255 (1996).
[18] E. Boos, M. Dubinin, A. Pukhov, M. Sachwitz, and H. J. Schreiber, Eur. Phys. J. C **21**, 81 (2001).
[19] F. Penunuri, F. Larios, and A. O. Bouzas, Phys. Rev. D **83**, 077501 (2011).
[20] C. Schwinn, arXiv:hep-ph/0412028.
[21] J. Fuster, I. Garcia, P. Gomis, M. Perell, E. Ros, and M. Vos, Eur. Phys. J. C **75**, 223 (2015).
[22] J. A. Aguilar-Saavedra, M. C. N. Fiolhais, and A. Onofre, J. High Energy Phys. 07 (2012) 180.
[23] C. Englert and M. Russell, Eur. Phys. J. C **77**, 535 (2017).
[24] V. Khachatryan *et al.* (CMS Collaboration), J. High Energy Phys. 02 (2017) 028.
[25] K. Kolodziej, Phys. Lett. B **584**, 89 (2004).
[26] Q. H. Cao and B. Yan, Phys. Rev. D **92**, 094018 (2015).
[27] P. Batra and T. M. P. Tait, Phys. Rev. D **74**, 054021 (2006).
[28] S. Liebler, G. Moortgat-Pick, and A. S. Papanastasiou, J. High Energy Phys. 03 (2016) 099.
[29] F. Bach and T. Ohl, Phys. Rev. D **86**, 114026 (2012).
[30] B. Ananthanarayan, J. Lahiri, M. Patra, and S. D. Rindani, Phys. Rev. D **86**, 114019 (2012).
[31] L. Chen, O. Dekkers, D. Heisler, W. Bernreuther, and Z. G. Si, J. High Energy Phys. 12 (2016) 098.
[32] J. Alwall, R. Frederix, S. Frixione, V. Hirschi, F. Maltoni, O. Mattelaer, H.-S. Shao, T. Stelzer, P. Torrielli, and M. Zaro, J. High Energy Phys. 07 (2014) 079.
[33] R. Brun and F. Rademakers, Nucl. Instrum. Methods Phys. Res., Sect. A **389**, 81 (1997).
[34] S. Chatrchyan *et al.* (CMS Collaboration), J. Instrum. **8**, P04013 (2013).
[35] C. Escobar (ATLAS and CMS Collaborations), arXiv:1709.02749.
[36] R. R. Aguilar, A. O. Bouzas, and F. Larios, Phys. Rev. D **92**, 114009 (2015).
[37] N. Castro, J. Erdmann, C. Grunwald, K. Krninger, and N. A. Rosien, Eur. Phys. J. C **76**, 432 (2016); J. L. Birman, F. Deliot, M. C. N. Fiolhais, A. Onofre, and C. M. Pease, Phys. Rev. D **93**, 113021 (2016); Z. Hioki, K. Ohkuma, and A. Uejima, Phys. Lett. B **761**, 219 (2016); V. Cirigliano, W. Dekens, J. de Vries, and E. Mereghetti, Phys. Rev. D **94**, 034031 (2016); I. Brivio, arXiv:1710.01003.
[38] A. Buckley, C. Englert, J. Ferrando, D. J. Miller, L. Moore, M. Russell, and C. D. White, J. High Energy Phys. 04 (2016) 015; Phys. Rev. D **92**, 091501 (2015).
[39] K. Skovpen (CMS Collaboration), arXiv:1711.02153.
[40] M. Aaboud *et al.* (ATLAS Collaboration), J. High Energy Phys. 12 (2017) 017; Eur. Phys. J. C **77**, 264 (2017).
[41] M. S. Amjad *et al.*, Eur. Phys. J. C **75**, 512 (2015).
[42] J. A. Aguilar-Saavedra, Nucl. Phys. **B821**, 215 (2009).
[43] A. Alloul, N. D. Christensen, C. Degrande, C. Duhr, and B. Fuks, Comput. Phys. Commun. **185** (2014) 2250.